A Bioinspired Alginate-Gum Arabic Hydrogel with Micro-/Nanoscale Structures for Controlled Drug Release in Chronic Wound Healing

Mi Li[†,⊥,∇,iD], **Haichang Li**[‡,∥,∇], **Xiangguang Li**[‡,∥,#], **Hua Zhu**[‡,∥], **Zihui Xu**[†], **Lianqing Liu**[*,⊥,iD], **Jianjie Ma**[*,‡,∥], and **Mingjun Zhang**[*,†,‡,§,iD]

[†]Department of Biomedical Engineering, College of Engineering, Columbus, Ohio 43210, United States

[‡]Dorothy M. Davis Heart & Lung Research Institute, Wexner Medical Center, Columbus, Ohio 43210, United States

[§]Interdisciplinary Biophysics Graduate Program, Columbus, Ohio 43210, United States

[∥]Department of Surgery, The Ohio State University, Columbus, Ohio 43210, United States

[⊥]State Key Laboratory of Robotics, Shenyang Institute of Automation, Chinese Academy of Sciences, Shenyang 110016, China

[#]College of Animal Science, South China Agricultural University, Guangzhou 510642, China

Abstract

Biopolymeric hydrogels have drawn increasing research interest in biomaterials due to their tunable physical and chemical properties for both creating bioactive cellular microenvironment and serving as sustainable therapeutic reagents. Inspired by a naturally occurring hydrogel secreted from the carnivorous Sundew plant for trapping insects, here we have developed a bioinspired hydrogel to deliver mitsugumin 53 (MG53), an important protein in cell membrane repair, for chronic wound healing. Both chemical compositions and micro-/nanomorphological properties inherent from the natural Sundew hydrogel were mimicked using sodium alginate and gum arabic with calcium ion-mediated cross-linking. On the basis of atomic force microscopy (AFM) force measurements, an optimal sticky hydrogel scaffold was obtained through orthogonal experimental design. Imaging and mechanical analysis showed the distinct correlation between structural morphology, adhesion characteristics, and mechanical properties of the Sundew-inspired

[*]**Corresponding Authors** lqliu@sia.cn, jianjie.ma@osumc.edu, Tel.: (614) 292-3181. Fax: (614) 292-7301. zhang.4882@osu.edu.
[∇]M.L. and H.L. contributed equally to this work.
ORCID
Mi Li: 0000-0002-8379-0057
Lianqing Liu: 0000-0002-9136-2458
Mingjun Zhang: 0000-0002-1004-8927

hydrogel. Combined characterization and biochemistry techniques were utilized to uncover the underlying molecular composition involved in the interactions between hydrogel and protein. In vitro drug release experiments confirmed that the Sundew-inspired hydrogel had a biphasic-kinetics release, which can facilitate both fast delivery of MG53 for improving the reepithelization process of the wounds and sustained release of the protein for treating chronic wounds. In vivo experiments showed that the Sundew-inspired hydrogel encapsulating with rhMG53 could facilitate dermal wound healing in mouse model. Together, these studies confirmed that the Sundew-inspired hydrogel has both tunable micro-/nanostructures and physicochemical properties, which enable it as a delivery vehicle for chronic wounding healing. The research may provide a new way to develop biocompatible and tunable biomaterials for sustainable drug release to meet the needs of biological activities.

Graphical Abstract
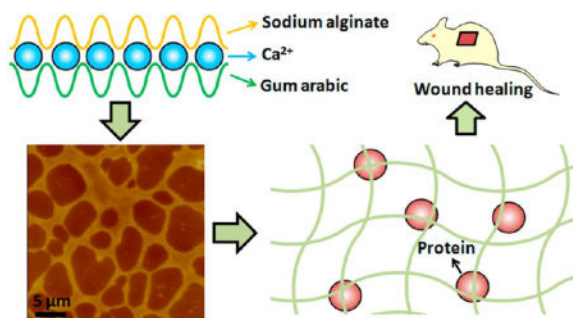
Keywords

bioinspired hydrogel; alginate and gum arabic; atomic force microscopy (AFM); drug release and delivery; recombinant human MG53 protein (rhMG53); wound healing and scarring

1. INTRODUCTION

Hydrogels are often composed of a large amount of water (typically 70–99%) and cross-linked polymer networks.[1] In recent years, various hydrogel products have been proposed in clinical applications (e.g., soft contact lenses, wound dressings, and biological adhesives in surgical procedures). Many new potential applications (e.g., stem cell and cancer research, cell therapy, tissue engineering, immunomodulation, and in vitro diagnostics) for hydrogels have also emerged.[2] A wide range of polymeric compositions have been proposed to fabricate hydrogels. In general, the polymer compositions can be divided into natural polymer hydrogels, synthetic polymer hydrogels, and combinations of the both.[3] Natural polymers are advantageous in their biocompatibility, cost, and gelation ability by addition of divalent cations.[4] Alginate, a widely used natural polymer for hydrogel, is a family of linear polysaccharides containing blocks of (1,4)-linked β-D-mannuronic acid (M) and a-L-guluronic acid (G) residues. The G-blocks participate in intermolecular cross-linking with divalent cations (e.g., Ca^{2+}) to form hydrogels.[5] Alginate hydrogels can be engineered to release small molecules and proteins, present bioactive ligands to cells, and degrade at a tunable rate.[6] However, alginate hydrogels have limited stretchability (alginate hydrogel

ruptures when stretched to about 1.2 times its original length) and are often brittle. In 2012, Sun et al.[7] fabricated a stretchable and tough hydrogel by mixing ionically cross-linked alginate and covalently cross-linked polyacrylamide. Besides, nanoparticles have been integrated into the hydrogel to enhance the adhesion and mechanical properties.[8,9] It is evident that designing hydrogels with enhanced mechanical properties to provide additional functionalities could play an important role in biomedical applications of the hydrogel. For example, fibrous and viscoelastic hydrogels that accurately recreate the complex structural and mechanical milieus found in tissues[10] are emerging as useful cell culture substrates.

For some applications, such as sealants for corneal wound, surgical adjuvant, and wet adhesives,[11] the adhesion capability becomes a crucial factor in determining the performance of the hydrogels. During the past decade, there has been substantial progress in developing several adhesive hydrogels inspired by natural bioadhesion phenomenon, such as the footpads of a gecko,[12] the adhesive used by mussels and ivies to cling to rocks,[13,14] nanofibrous structures used by tunicates to heal damage,[15] the proboscis used by endoparasite *pomphorhynchuslaevis*,[16] and the noncovalent interactions involved in various biological processes including cell adhesion to extracellular biomolecules or bacterial adhesion.[17] Mimicry is being used in the design of adhesive polymers for biomedical applications that are required locally in tissues, systematically throughout the body, and at the interface with tissues.[18]

Sundew, a carnivorous plant, catches its prey by secreting sticky mucilage on the leaves' surface.[19] Studies have shown that the mucilage produced by Sundew is a viscoelastic and homogeneous polysaccharide (with a molecular weight over 2×10^6 Da) aqueous solution (the concentration is about 4%).[20] Gum arabic is a natural biopolymer inheriting complex and branched polymeric structures, which confers high cohesive and adhesive properties.[21] These properties make gum arabic widely used in the food industry (as dietary fiber)[22] and pharmaceutical preparations (as suspending agent, emulsifying agent, binder in tablets, demulcent, and emollient in cosmetics).[21] In the present work, Sundew-inspired hydrogels with tunable physical properties (structures, mechanical properties, and adhesion characteristics) have been developed using sodium alginate and gum arabic with calcium-mediated cross-linking, showing that the fabricated Sundew-inspired hydrogels had well-patterned scaffold structures that are similar to that of the natural scaffolds from Sundew mucilage. Atomic force microscopy (AFM)[23] was used to characterize structural topography and adhesion force of the fabricated hydrogels. Through orthogonal experimental design, the component ratios were optimized to achieve a hydrogel with enhanced adhesion characteristics.

MG53, a tripartite motif (TRIM) family protein, has been identified as an essential component of cell membrane repair machinery.[24] Our previous study has shown that topical application of the recombinant human (rh) MG53 protein can promote wound healing with reduced scarring.[25] MG53 is capable of nucleating the membrane repair machinery in keratinocytes, which therefore repairs injuries to the epidermis. MG53 presenting in the extracellular solution can facilitate migration of fibroblasts and keratinocytes in response to scratch wounding, thus contributing to efficient reepithelization of wound closure. However, therapeutic efficacy of the rhMG53 depends on the formulation and delivery approach.

Because of the short half-life of MG53 in circulation, sustained release of rhMG53 at the wound site is expected to have a higher efficacy and thus is more clinically attractive. In this study, the Sundew-inspired hydrogel was used to encapsulate MG53 protein for chronic wound healing. The Sundew-inspired hydrogel has been tested for biocompatible and was confirmed on less concern for immunogenicity; it can modulate both quick and sustained delivery of rhMG53 to facilitate healing of dermal wounds in rodent models.

2. MATERIALS AND METHODS

2.1. Materials

Sodium alginate, gum arabic, and calcium chloride dihydrate were purchased from Sigma-Aldrich (St. Louis, MO). rhMG53 (2 mg/vial) was obtained from TRIM-edicine Co. (Columbus, OH). Coverslips (25 mm × 25 mm) were purchased from Thermo Fisher Scientific (Waltham, MA). Pure water produced by Barnstead Nanopure (Thermo Fisher Scientific, Waltham, MA) was used. Dulbecco's phosphate buffered saline (DPBS) was purchased from Gibco by life technologies (Waltham, MA). The dialysis membrane (molecular weight cutoff: 300 kDa) was purchased from Spectrum Laboratories (Rancho Dominguez, CA). Male C57BL6 mice were purchased from Jackson Laboratories (Bar Harbor, ME).

2.2. Sundew-Inspired Adhesive Hydrogel Fabrication

The adhesive hydrogel was fabricated through the cross-linking reaction of sodium alginate and gum arabic under calcium ion. (1) Prepare 1 M Ca^{2+} solution by dissolving 1.47 g of $CaCl_2 \cdot 2H_2O$ with 10 mL of pure water. (2) Pipette a certain amount of Ca^{2+} solution into 2 mL of pure water in a vial to prepare Ca^{2+} solution (e.g., 5, 10, 15 mM). (3) Add a certain amount of gum arabic powder (e.g., for fabricating hydrogels containing 3% (w/v) gum arabic, 60 mg of gum arabic powder was added) into the vial, and then stir the solution using a magnetic stirrer (Corning, New York) until the gum arabic is fully dissolved. (4) Add a certain amount of sodium alginate (e.g., for hydrogels containing 3% (w/v) sodium alginate, 60 mg of sodium alginate was added) into the vial and then stir for about 1 h to obtain the fabricated hydrogel. (5) Take the magnetic rotor from the vial and then pour the hydrogels into a centrifuge tube. The fabricated hydrogels were stored at 4 °C for avoiding microbial contamination.

The rhMG53-packed hydrogel was prepared according to the following procedure. (1) Dissolve 2 mg of rhMG53 powder with 2 mL of pure water in a vial. (2) Pipette a certain Ca^{2+} solution into the vial. (3) Gum arabic powder was added into the vial under magnetic stirring. (4) After the gum arabic is fully dissolved, sodium alginate was added into the vial under magnetic stirring to form hydrogels. For simplicity, the hydrogel containing X% sodium alginate (SA), Y% gum arabic (GA), and Z mM Ca^{2+} will be abbreviated as hydrogel (X-Y-Z).

2.3. Atomic Force Microscopy

AFM experiments were performed with a MFP-3D AFM (Oxford Instruments Asylum Research, Santa Barbara, CA), which was set on a FV1000 inverted microscope (Olympus,

Shinjuku, Tokyo, Japan) . The conical silicon nitride probe (NanoWorld, Neuchatel, Switzerland) with a nominal spring constant of 0.08 N/m was used for imaging. The spherical probe (a gold sphere was attached to a silicon cantilever) (NanoAndMore GmbH, Watsonville, CA) with a nominal spring constant of 2.8 N/m was used for force measurements.

After pipetting a drop of hydrogel onto a fresh coverslip (i), another coverslip (ii) was used to press the hydrogel to make it spread on the coverslip (i) and then scratch the hydrogel to form a thin layer on the coverslip (i). The coverslip (i) containing hydrogel layer then were glued onto a glass slide, which was then placed at the sample stage of AFM and AFM experiments were immediately performed. With the help of an optical microscope, the AFM probe was controlled to approach the hydrogel, after which AFM imaging and force measurements were performed. Before AFM experiments, the probe was calibrated. First, the deflection sensitivity of the cantilever was calibrated at a bare area on the coverslip. Next, the spring constant of the cantilever was calibrated by thermal noise method.[23]

AFM images were recorded at contact mode at room temperature. The scan line was 256 and the sampling point for each scan line was also 256. The imaging rate was 0.3 Hz. Both height image and deflection image were recorded. To measure the adhesion forces of the hydrogels, force curves were recorded on different areas of the hydrogel-coated coverslip at force volume mode. For each $35 \times 35\ \mu m^2$ area, 32×32 force curves were recorded at relative trigger mode. The ramp size was 1 μm, and the loading velocity of tip was 2 μm/s. The trigger threshold for conical tip was 10 nN, and the trigger threshold for spherical tip was 100 nN. During the force volume mode, both topography image and adhesion force map were recorded. The adhesion force maps were automatically acquired by the Asylum software (Oxford Instruments Asylum Research, Santa Barbara, CA).

2.4. Scanning Electron Microscopy

For scanning electron microscopy (SEM) of the fabricated hydrogels, a fresh coverslip was coated by a thin layer of the hydrogel (3-3-15). The coverslip was then coated by a layer of gold with thickness of 25 nm. The coverslip then was scanned by a Nova NanoSEM (FEI Co., Hillsboro, OR) to obtain the images of the hydrogel.

2.5. Rheological Measurements

Rheological experiments were performed with an AR1000-N rheometer (TA Instruments, New Castle, DE). The 40 mm aluminum parallel plate was used for measurements. The nitrogen pressure required for the rheometer was 25 psi, and the gap between sample stage and plate for measurements was 500 μm. Hydrogels with different component ratios were placed directly on the sample stage of the rheometer at room temperature. Frequency sweeps (the angular frequency of the plate was from 6.28 to 62.77 rad/s) were performed to determine the values of the storage modulus (G') and loss modulus (G'').

2.6. In Vitro Protein Release Studies

Hydrogels packing rhMG53 was loaded into the dialysis membrane, which was then immersed in 10 mL of DPBS ($1\times$) in a vial. The medium in the vial was mixed with a

magnetic stirrer at room temperature. At definite time intervals, 0.3 mL of the release medium was collected and stored at 4 °C for avoiding microbial contamination. Next, 0.3 mL of fresh DPBS was added into the vial. The concentration of rhMG53 in the collected samples was measured by using a DU 800 spectrophotometer (Beckman Coulter, Fullerton, CA). 280 nm wavelength was used. The standard curve was obtained by measuring the absorbance of a series of rhMG53 concentrations in DPBS (0, 0.01, 0.125, 0.25, 0.375, 0.5, 0.625, 0.75, and 1 mg/mL). The standard curve was linearly fitted. According to the fitted curve, the MG53 concentration for each collected sample was calculated. The cumulative release ratio of MG53 was determined by dividing the amount of released MG53 by the amount of MG53 packed in the hydrogels:

$$R_n = \frac{V_c \sum_1^{n-1} C_i + V_0 C_n}{m} \times 100 \% \quad (1)$$

where R_n is the cumulative release of the nth sample collection, m is the overall MG53 in the hydrogel loaded in the dialysis membrane, C_n is the MG53 concentration of the nth sample collection, V_0 is the volume of the overall release medium in the vial ($V_0 = 10$ mL), V_c is the volume of the sample collected each time ($V_c = 0.3$ mL), and C_i is the MG53 concentration of the ith sample.

2.7. Confocal Fluorescence Microscopy

For fluorescence imaging, rhMG53 was conjugated with red fluorescein by an Alexa Fluor 647 protein labeling kit (Life Technologies Corp., Eugene, OR). Next, Alexa 647-labeled MG53 was packed in hydrogels. The hydrogel was directly dropped onto a Petri dish, which was then placed at the sample stage of a LSM 780 laser confocal fluorescence microscope (Zeiss, Oberkochen, Germany). The bright field images and corresponding fluorescence images then were simultaneously recorded.

2.8. Dynamic Light Scattering

The zeta potential distribution of particles in gum arabic was measured by dynamic light scattering (DLS) at 25 °C using a Zetasizer Nano (Malvern Instruments Ltd., Malvern, UK). 6% (w/v) gum arabic was prepared by dissolving 120 mg of gum arabic powder in 2 mL of pure water. A certain amount of Ca^{2+} solution was pipetted into the gum arabic solution to prepare pure water solution containing 6% gum arabic and 20 mM Ca^{2+}. The gum arabic solution with and without Ca^{2+} then was diluted to one tenth with pure water. The samples were then measured by DLS.

2.9. In Vivo Animal Studies

Animal studies followed the guidelines of the National Institutes of Health and were approved by the ethical committee of The Ohio State University. The experimental steps of mice wound healing studies were performed according to the previously established procedure.[25] Surgical excision wounds were created as detailed below. For pain management, all animals received drinking water containing 200 mg/L ibuprofen (Precision Dose Inc., South Beloit, IL) for 2 days prior to and 5 days postsurgery.

The dorsal hair of the mice was shaved using an electric clipper, and the naked skin areas of the mice were wiped by betadine solution to avoid infection. Alcohol prep pads then were used to wipe the naked skin areas. Two full thickness dermal wounds (3 cm apart and 4 cm caudal to the scapulae) were created using sterile 6 mm-diameter biopsy punches (Integra Miltex, Plainsboro, NJ) to expose the underlying dorsolateral skeletal muscle fascia. Hemostasis was achieved by even compression with sterile gauze. Wounds were left open with no dressing and then immediately received a subcutaneous injection of either 200 μL of PBS saline (as control) or rhMG53 (1 mg/kg), Sundew-inspired hydrogel, and Sundew-inspired hydrogel encapsulating rhMG53. The Sundew-inspired hydrogel (6-4-20) was used. The concentration of MG53 encapsulated in the hydrogel was 0.2 mg/mL.

A digital camera (Panasonic, Kadoma, Osaka, Japan) was used to capture the wound with a metric ruler inside the field of view used to set scale for measurements. The wound bed was measured using a digital caliper (CD-6″CSX, Mitutoyo Corp., Japan). Blinded measurement of wound size was performed using ImageJ software. The perimeter of the wound was then traced, and the wound area was recorded. Wound size on day 0 was set to 100%, and each subsequent day was reported as a percentage of initial wound size.

2.10. Histology and Immunohistochemistry

Histology and immunohistochemistry studies were performed as described previously.[25] Briefly, skin, heart, liver, spleen, lung, and kidney samples dissected from experimental animals were fixed in 4% paraformaldehyde overnight at 4 °C. Skin samples were pinned to styrofoam rafts to maintain morphology during the fixation. After fixing, samples were washed three times for 5 min with 70% ethanol. Washed samples were then processed, and embedded in paraffin. Four micrometer thick paraffin sections were cut and stained with Hematoxylin-Eosin (H&E) and Masson's trichrome.

Immunohistochemical staining was carried out using F4/80 antibody (Santa Cruz Biotechnology, Dallas, TX) with the above skin tissues. Alexa 546-conjugated goat antirabbit IgG (Molecular Probes, Eugene, OR) was used for labeling of skin sections that were positive for F4/80 staining. Images were taken and analyzed using a Zeiss 780 confocal microscope (Zeiss, Oberkochen, Germany).

Measurement of the skin thickness at wound site was performed using ImageJ software with Masson's trichrome staining on the skin samples dissected from the mice treated with saline, rhMG53, Sundew-inspired hydrogel, or Sundew-inspired hydrogel encapsulating rhMG53 30 days after an injury.

2.11. Statistical Analysis

All data are presented as means ± SD. Groups were compared by student t tests and by ANOVA for repeated measures. A value of $P < 0.05$ was considered significant.

3. RESULTS AND DISCUSSION

3.1. Fabrication of the Sundew-Inspired Adhesive Hydrogel

The sticky mucilage secreted by Sundew plant is produced by the stalked glands (also so-called tentacles) on the leaves' surface,[19] as shown in Figure 1A and B. Upon the prey touching the mucilage-covered glands, the prey will be easily trapped in the mucilage. The gland then secretes enzymes to digest the prey and absorb the nutrients through the leaf surfaces.[27] A notable feature of the Sundew mucilage is that it is very sticky, which helps the Sundew to capture the prey (inset in Figure 1B). The Sundew mucilage is a single polysaccharide solution,[20] and AFM imaging of the Sundew mucilage shows that the mucilage has well-defined porous scaffolds (Figure 1C). As shown in Figure 1D, the main components of the Sundew mucilage are arabinose, galactose, mannose, glucuronic acid, and inorganic cations (22 mM Ca^{2+}).[20,28] The backbone of the polysaccharide is a repeating dimer of glucuronic acid and mannose, and the other sugars are present in end groups and side chains. Alginates are polysaccharides that are rich in mannuronic acid and guluronic acid.[4] Gum arabic is a commonly used hydrocolloid in the food industry due to its excellent emulsifying properties.[29] Gum arabic mainly contains arabinogalactan, which accounts for ~88% of the total gum.[29] Hence, alginate and gum arabic were used to mimic the Sundew mucilage. Figure 1E shows the schematic drawing of the formation of Sundew-inspired adhesive hydrogels, which have patterned structures. Sodium alginate cross-links with gum arabic via Ca^{2+} to form Sundew-inspired hydrogel. AFM topography images revealed the porous scaffold structures of the fabricated hydrogel, while the adhesion characteristics of the fabricated hydrogel were sensed by touching and pulling a drop hydrogel between two fingers. Figure S1A is a drop of the fabricated Sundew-inspired hydrogel on a coverslip, showing the hydrogel with milky color. After a layer of fabricated Sundew-inspired hydrogel was coated on a Petri dish, a hydrogel sheet was obtained by peeling it off the Petri dish when the water in the hydrogel evaporated, as shown in Figure S1B.

3.2. Component Ratio Optimization To Achieve Enhanced Adhesion Characteristics for the Sundew-Inspired Hydrogel

Figure 2 shows adhesion characteristics of the fabricated Sundew-inspired hydrogels by AFM. To obtain a force curve, the AFM probe was controlled to perform an approach-retract cycle in the vertical direction on the substrate.[30] Researchers have widely used AFM force spectroscopy to investigate the adhesion forces of adhesives, such as DOPA polymer adhesive,[12] adhesive mimicking gecko foot-hair,[31] carbohydrate hydrogel,[32] and alginate hydrogel.[33] Here, we used the AFM to characterize the adhesion characteristics of the fabricated Sundew-inspired hydrogel. Figure 2A is a representative force curve obtained on the hydrogel-coated substrate with conical tip, showing that the adhesion force was about 20 nN. For some hydrogels, the adhesion forces between hydrogels and AFM tip were large and exceeded the measurement range of the cantilever with conical tip (Figure S2). To measure the adhesion force of these hydrogels, cantilever with spherical tip was used. A representative force curve obtained by the spherical tip is shown in Figure 2B, showing that the adhesion force was about 150 nN. During the force volume mode, the topography image and adhesion force map of the hydrogel-coated substrate were simultaneously obtained. Figure 2C shows a representative topography image, and Figure 2D is the corresponding

adhesion force map recorded by conical tip. Network porous scaffold structures were clearly discerned in the topographic image, while the adhesion force map showed that there were no significant differences in the adhesion forces between scaffold area (denoted by the red asterisks) and blank area (denoted by the white asterisks). Figure 2E is the statistical histogram of the adhesion forces in Figure 2D, showing that the adhesion forces could be well fitted by Gaussian function. Figure 2F–H shows the results obtained with a spherical tip, and also shows the porous scaffold structures of the hydrogel with no significant differences in the adhesion forces between scaffold area and blank area.

To explore the different adhesion forces between scaffold area and blank area, control experiments were performed, as shown in Figure 2I–K. With the same spherical tip, adhesion force maps were first obtained on control substrate (without hydrogel) (Figure 2I) and hydrogel-coated substrate (Figure 2J), showing that the adhesion force on hydrogel-coated substrate was significantly larger than that on the control substrate. The same tip then was used to measure the adhesion force on the control substrate again (Figure 2K), showing that the adhesion force significantly decreased to the level comparable to the adhesion force in Figure 2I. During the experiments, hydrogels on the substrate may adhere to the AFM tip, which may influence the force measurements. However, the results in Figure 2I–K showed that this effect (hydrogel adhering to AFM tip) was weak. Further, AFM images of the hydrogel-coated substrate were obtained, as shown in Figure 2L,M. We can see that there were many nanoparticles in the blank area of the hydrogel (denoted by the blue asterisks). This indicated that the blank area of the hydrogel on the substrate was coated by nanoparticles, which caused that the adhesion force on the blank area of the hydrogel was comparable to that on the scaffold area of the hydrogel. In fact, the following results show that the scaffold area of the hydrogel was also formed by nanoparticles. By AFM force volume mode, the topography image and adhesion force map can be simultaneously recorded, which is useful for investigating the underlying relationships between the structures and adhesion characteristics of the adhesive hydrogels.

By AFM force spectroscopy, a conical tip was used to investigate the adhesion forces of hydrogels in two different states: wet and dried, as shown in Figure S3. For measuring the adhesion forces of wet hydrogels, AFM measurements were immediately performed after coating a layer of fabricated hydrogel on the coverslip. For measuring the adhesion forces of dried hydrogels, the hydrogel coated on the coverslip dried in air for about 4 h, and then AFM measurements were performed. Figure S3A is the histogram of adhesion forces of 10 dried hydrogels, and Figure S3B is the corresponding adhesion forces of the 10 hydrogels in wet status. They all clearly show that the adhesion forces of hydrogels in wet status were significantly larger than those in dried status. Figure S3C is the dynamic changes of adhesion forces on the same hydrogel-coated substrate area, showing that the adhesion force decreased from about 23 to about 12 nN in 90 min in air at room temperature. The experimental results (Figure S3) indicated that the different status (wet, dried) can influence the adhesion force of the hydrogel, and thus in the subsequent experiments AFM force measurements were performed on wet hydrogels to maintain the identical conditions for all hydrogels.

As compared to conventional nonadhesive hydrogels, adhesive hydrogels are advantageous in many applications, such as wound closure,[34] tissue healing,[35] cell spreading,[36] and tissue regeneration.[37] On the one hand, adhesive hydrogels can bind various tissues together to allow proper healing to occur, control or stop the bleeding, or prevent gas or fluid leakage from the tissue by acting as an adhesive, hemostat, or sealant, respectively.[34] On the other hand, adhesive hydrogels facilitate cell adhesion and migration on it, which can promote cell proliferation and differentiation.[38] Hence, we optimized the adhesion characteristics of the sundew-inspired adhesive hydrogels via orthogonal experimental design, as shown in Figure 3. The detailed bar values and orthogonal analysis of Figure 3A–D are shown in Tables S1–S4, respectively. Figure 3A shows the results of $L_{25}(5^3)$ orthogonal experiments, during which five levels for each of the three component were tested. The statistical histogram of the adhesion forces (Figure 3Ai) showed that the hydrogel (3-3-15) had the largest adhesion force, whereas orthogonal analysis predicted that the hydrogel (3-2-15) had the largest adhesion force (Figure 3Aii). We then fabricated the hydrogel (3-2-15), and AFM measurement showed that its adhesion force (37 ± 3 nN) was smaller than the adhesion force (58 ± 4 nN) of the hydrogel (3-3-15). Figure 3Aiii shows that the importance order of the three components to the adhesion force of the hydrogels was SA > Ca^{2+} > GA. Figure 3B is the results of another $L_{25}(5^3)$ orthogonal experiment, during which five higher levels for each component were tested. In this case, the histogram of adhesion forces (Figure 3Bi) showed that several hydrogels (e.g., 3-3-9, 3-7-21, 4-6-21, and 6-7-15) had similar larger adhesion forces than the remaining hydrogels. Orthogonal analysis predicted that the hydrogel (6-7-21) had the largest adhesion force (Figure 3Bii). We then fabricated this hydrogel, and the AFM measurement showed that its adhesion force (44 ± 2 nN) was slightly larger than those of all of the tested hydrogels in Figure 3B. The important order for the adhesion forces of the hydrogels was Ca^{2+} > SA > GA (Figure 3Biii). We then performed orthogonal experiments on hydrogels containing higher levels of SA, GA, and Ca^{2+}. Yet the adhesion forces of these hydrogels were not measurable by conical tip (as shown in Figure S2), and thus we used a spherical tip to measure the adhesion forces of these hydrogels. For control, we first used a spherical tip to measure the representative four hydrogels that had been tested by conical tip, and the results are shown in Figure 3C. We can see that the hydrogel (6-7-21) had the largest adhesion force as compared to the other three hydrogels. The spherical tip then was used to investigate the adhesion forces of hydrogels containing higher levels of the components, and the results are shown in Figure 3D. $L_9(3^3)$ orthogonal experiments were designed, during which three levels for each component were tested. The experimental results (Figure 3Di) showed that the hydrogel (7-8-27) had the largest adhesion force, whereas the orthogonal analysis (Figure 3Dii) predicted that the hydrogel (8-8-27) had the largest adhesion force. We then fabricated this hydrogel and measured the adhesion force (133 ± 37 nN), which was smaller than the adhesion force (228 ± 81 nN) of the hydrogel (7-8-27). The order for the adhesion forces of the hydrogels was SA > Ca^{2+} > GA.

The orthogonal results in Figure 3 indicated that sodium alginate and Ca^{2+} are more important than gum arabic in mediating the adhesion forces of the hydrogels. Besides, different combinations of the three components (SA, GA, and Ca^{2+}) can lead to the different adhesion forces of the fabricated hydrogels. Overall, the increase of the concentrations of the

three components can lead to higher adhesion forces, but the increase of the adhesion forces versus the concentrations of the components was not linear. There are some local maximal adhesion forces in certain combinations (e.g., 3-3-15, 6-7-21, and 7-8-27). To compare the adhesion force of the fabricated hydrogels with that of the mucilage secreted by Sundew, the adhesion force of the Sundew mucilage was measured. Mucilage secreted by Sundew was collected by pipet and dropped onto the coverslip. Force curves then were obtained on the mucilage-coated coverslip (see Figure S4). The results showed that the adhesion force of the Sundew mucilage (Figure 3E) was comparable to the adhesion force of the fabricated Sundew-inspired hydrogel (Figure 3C,D).

3.3. Structural Morphology and Mechanical Properties of the Sundew-Inspired Hydrogel

Figure 4 shows the structural morphology and mechanical properties of the Sundew-inspired hydrogels. Ten representative Sundew-inspired hydrogels were imaged by AFM. The optical bright field images of the hydrogels were shown in Figure S5. For the hydrogel (1-1-5), the network scaffold structures were not visible in the bright field image (Figure S5), but membrane-containing micropores were discerned in the AFM image (Figure 4A). For the hydrogel (2-2-10) (Figure 4B) and the hydrogel (3-3-15) (Figure 4C), the cross-linked network porous scaffold structures were clearly visible in both AFM height and bright field images. When the component ratio became (4-5-20) (Figure 4D), although there were scaffold structures in the hydrogel, the scaffold structures were relatively thin and some scaffolds distributed discretely (denoted by the red arrow in Figure 4D). Besides, many nanoparticles with different sizes in the nonscaffold areas were observed in the AFM image (denoted by the red asterisks in Figure 4D). For the hydrogel (6-4-20) (Figure 4E), the cross-linked network porous scaffold structures were clearly visible in both the AFM image and bright field image again. For the hydrogel (6-7-21), thick scaffold structures were observed (Figure 4F), but were relatively discrete (Figure S5). When the concentrations of the three components further increased (Figure 4G–J), there were no cross-linked network scaffold structures except the particles with different sizes. To investigate the relationships between the three components and the network porous scaffold structures, AFM images were obtained on control groups, as shown in Figure S6. The control experiments were designed for the hydrogel (3-3-15). For the control experiments, only two components were dissolved together in pure water. We can clearly see that none of the three control groups (Figure S6) showed the network scaffold structures as observed in Figure 4C, demonstrating that the formation of network scaffold structures required the participation of SA, GA, and Ca^{2+} (as shown in the schematic diagram in Figure 1E).

Conventional methods for visualizing the detailed network structures of hydrogels are based on scanning electron microscopy (SEM) imaging.[39–42] Here, we also used SEM to visualize the topography of the hydrogel (3-3-15), and a typical SEM image is shown in Figure 4K. More SEM images are shown in Figure S7. From SEM images, we can see clearly see the scaffold of the hydrogel. The nanoparticles are also visible (denoted by the red asterisks in Figure 4K). Hence, the SEM results verified the results of AFM imaging (Figure 4C). Combining the morphology results of Figure 4 with the adhesion force in Figure 3, we can see that hydrogels possessing higher adhesion forces have well-patterned network scaffold structures, such as the hydrogel (3-3-15) (Figure 3Ai and Figure 4C) and the hydrogel

(6-7-21) (Figure 3C and Figure 4F). For the hydrogels containing higher levels of the components (e.g., 7-8-27, 8-7-27, 8-9-24, and 9-9-27), there were no network scaffold structures in these hydrogels (Figure 4G–J), and their adhesion forces were significantly smaller than the hydrogel (6-7-21), which had thick network structures (Figure 4F). Hence, the morphology results indicate the close links between the network scaffold structures and the adhesion characteristics of the hydrogels.

The mechanical properties of hydrogels are important for creating a microenvironment in supporting cellular activities.[43–46] For example, when hydrogels are used as biomaterials for cell growth matrix, its stiffness can significantly influence the differentiation of stem cells.[46] Besides, the mechanical properties of hydrogel-based extracellular matrix also impact cell motility, cell spreading, adult tissue homeostasis, and tumor metastasis.[47–49] Hence, we investigated the mechanical properties of the fabricated Sundew-inspired hydrogels, and the results are shown in Figure 4L,M. Nine hydrogels were measured. Figure 4L,M shows the storage modulus and loss modulus of the nine hydrogels, respectively. Storage modulus reflects the elastic deformation ability of the material, and loss modulus reflects the viscous deformation ability of the material. We can see that when the concentrations of hydrogel components (SA, GA, and Ca^{2+}) increased from (2-2-10) to (7-8-27), the storage modulus and loss modulus of hydrogels increased gradually, except the storage modulus of the combination (4-5-20). However, when the concentration of hydrogel components increased further to (8-7-27), (8-9-24), and (9-9-27), the storage modulus and loss modulus decreased significantly.

Combining the mechanical data with the structural data, we can observe that the mechanical properties of the fabricated hydrogels are influenced by several factors, such as component concentration and hydrogel structure. First, the concentrations of the components were to some extent related to the mechanical properties of the hydrogel. For example, the hydrogel (2-2-10) had the lowest concentration, and also possessed the weakest mechanical properties. When the concentration increased, the mechanical properties became stronger until the combination (7-8-27). The hydrogel (9-9-27) had the highest concentration, but had weak mechanical properties, showing that concentration was not the sole factor determining the mechanical properties of the hydrogels. Second, the structures of the hydrogels were also related to the mechanical properties of the hydrogels. For the hydrogels that had higher component concentrations but weaker mechanical properties (e.g., 8-9-24 and 9-9-27), they had no network scaffold structures, whereas others had well-patterned scaffold structures.

3.4. Encapsulating MG53 Proteins with the Sundew-Inspired Hydrogel

Cell membrane repair is a fundamental biological phenomenon in mammalian cells. Microbial cells are protected by a stiff and impermeable cell wall. For eukaryotic cells whose cell membrane are not protected by a cell wall, they have developed cell membrane repair mechanisms, which allow them to reseal their membrane to prevent the efflux of cytoplasmic constituents and the uncontrolled influx of calcium.[50] In fact, many human pathologies are characterized by membrane injury, and thus modulation of membrane repair pathways holds tremendous therapeutic potential.[51] Previously, Dr. Ma's laboratory identified a novel TRIM family protein, named MG53, as an essential component of the cell

membrane repair machinery.[24] Genetic ablation of MG53 results in defective membrane repair and tissue regenerative capacity.[52] The recombinant human MG53 (rhMG53) protein can protect against membrane disruption in various cell types, when applied to the extracellular environment, and ameliorate pathology associated with muscular dystrophy and lung injury.[53–56] The research team also showed that rhMG53 is effective in protecting against myocardial infarction[57] and acute kidney injury.[26] More recently, the team showed that MG53 is a vital component of wound healing and that topical application of the rhMG53 protein has potential to promote wound healing with reduced scarring.[25] Hence, MG53 is potentially therapeutic drug for injury treatment, and we explored encapsulating it with the Sundew-inspired hydrogel, as shown in Figure 5.

According to the results of orthogonal experimental results (Figure 3) and characterization results (Figure 4), five representative Sundew-inspired hydrogels were fabricated to encapsulate MG53 proteins (Figure 5A–E). Figure 5A shows the result of hydrogel (3-3-15), illustrating that rhMG53 proteins distributed evenly in the hydrogel. Figure 5B is the result of hydrogel (4-5-20), showing that MG53 proteins clustered in local reservoir areas (denoted by the arrows in Figure 5B) in the hydrogel and the reservoir areas were clearly visible from the corresponding bright field image. Figure 5C is the result of hydrogel (6-4-20), showing that the rhMG53 protein distributed in local reservoir areas but the size of the reservoir areas was significantly smaller than the size of the reservoir areas in Figure 5B. Figure 5D is the result of hydrogel (6-7-21), and Figure 5E is the result of the hydrogel (8-7-27). Both Figure 5D and E showed that MG53 distributed in local reservoir areas and the sizes of the reservoir areas were significantly larger than the size of the reservoir areas in Figure 5B,C.

The detailed morphology of the MG53-contained reservoir areas in the hydrogel was imaged by AFM. Reservoir areas were clearly visible from the optical bright images (Figure 5F,G), as denoted by the arrows in Figure 5F and circled in Figure 5G. AFM imaging (Figure 5H–J) showed that the reservoir areas adhered to the network scaffold structures of the hydrogel (the scaffold structures are denoted by the arrows in Figure 5I) and the reservoir areas were rougher than the scaffold structures. The nonreservoir areas of the scaffold were also imaged (Figure S8), showing that there were many nanoparticles on the scaffold structures (denoted by the arrows in Figure S8D) and the porous areas (denoted by the asterisks in Figure S8D). AFM images of the hydrogel without MG53 also revealed that there were many nanoparticles in the scaffold structures of the hydrogel (denoted by the arrows in Figure S8F) and in the porous areas (denoted by the asterisks in Figure S8F), indicating that particles widely distributed in the hydrogels. Both of the AFM images of the hydrogel without rhMG53 (Figure 4, Figures S8 and S9) and with rhMG53 (Figure 5) show the scaffold structures, nanoparticles, and reservoir structures. We cannot discern significant differences between the hydrogel structure with or without rhMG53.

The mechanisms involved in the formation of the hydrogel were explored. The optical and AFM images (Figure S9A–D) of the hydrogel without MG53 also showed many reservoir areas with rough surface, indicating that the formation of reservoir area in the Sundew-inspired hydrogel was independent of the MG53 proteins. Control experiments (Figure S9E–H) demonstrated that the formation of reservoir areas was dependent on SA and GA. Gum arabic is a type of polysaccharide emulsifier that is widely used for the production of

emulsion-based foods.[58] Gum arabic contains both protein and polysaccharide residues. The proteinaceous components of the gum can embed in the oil phase, while the carbohydrate ones can extend out from the surface into the aqueous phase.[59] Gum arabic can form droplet emulsion when mixed with other natural polysaccharides, such as chitosan.[60] Here, the mixture of gum arabic and alginate can result in the formation of reservoir areas in the hydrogel (Figure 5F). From Figure 2M and Figure S8D–F, we can see many nanoparticles in the hydrogels, and thus it is reasonable to hypothesize that the rough surface of the reservoir area may be related to the nanoparticles. We then applied AFM to image the detailed morphological structures of the reservoir areas, as shown in Figure 5K,L. Nanoparticles were remarkably discernible when the GA concentration increased (Figure 5L), indicating the relationship between GA and the particle structures of the reservoir areas of the hydrogel. We then directly used AFM to image the solution (0-6-20) on the coverslip (a drop of the solution was placed on the coverslip and dried in air), and the results (Figure 5M) showed the well-defined nanoparticles on the substrate, indicating that the solution of GA contained many particles. The solution containing higher concentrations of GA was also observed (Figure 5N), showing that larger particles were clearly visible and indicating that the GA nanoparticles could accumulate together to form larger particles. Figure 5O shows the zeta potential of the gum arabic particles in pure water solution. The detailed zeta potential distributions were shown in Figure S10. We can see that the gum arabic particles are negatively charged. The addition of positive charges of Ca^{2+} could balance some negative charges of gum arabic nanoparticles. Sodium alginate is negatively charged in water.[4] Hence, the fabricated Sundew-inspired hydrogels were negatively charged. MG53 proteins are positively charged,[26] and thus they can bind to the GA particles. It should be noted that there were few nanoparticles in Figure S6B, but there were many nanoparticles in Figure 5M. This is because Figure S6B was obtained by dropping GA solution onto a coverslip and then placing another coverslip on the drop to form a thin layer on the coverslip, causing few nanoparticles to be observed in the AFM image. Figure 5M was obtained by dropping GA solution onto a coverslip without placing another coverslip on the drop, so that many nanoparticles aggregated in the local areas and thus nanoparticles were observed. Collectively, the experimental results (Figure 5) indicate that during the formation of the hydrogels, MG53 proteins bind to GA particles via electrostatic adsorption. The GA particles then cross-link with SA molecules via Ca^{2+} to form network scaffold structures. The redundant GA particles lead to the formation of reservoir areas trapped by the scaffold structures in the hydrogels.

3.5. In Vitro Drug Release and Degradation of the Sundew-Inspired Hydrogel

We have investigated the release of MG53 encapsulated in the hydrogels and the hydrogel degradation by in vitro experiments. Figure 6A,B shows the in vitro release experiments of the MG53-encapsulated hydrogels. Three representative hydrogels were fabricated, including (3-3-15), (6-4-20), and (7-8-27). From Figure 6A, we can see that in 8 days the release of rhMG53s in the hydrogel (6-4-20) was the highest, and the release of MG53s in the hydrogel (3-3-15) was the lowest. Burst release was observed in the first 4 h. After 4 h, the release of MG53 in the hydrogel (7-8-27) was higher than that in the hydrogel (6-4-20). Yet after 24 h, the release in the hydrogel (6-4-20) became higher than that in the hydrogel (7-8-27). The dominant mechanisms governing the protein release from hydrogels are

diffusion and degradation.[61] When the hydrogel pores are bigger than the radius of the protein, diffusion is the driving mechanism for release, and degradation is the main mechanism for release when the hydrogel pores are smaller than the radius of the protein.[62] Thus, the bioinspired hydrogel displayed a biphasic kinetics of rhMG53 release; it can facilitate fast delivery of the protein for improving reepithelization of the wounds, as well as release the protein in a sustained fashion for treating the remodeling phase of chronic wounds, which is critically needed.

To observe the dynamic degradation of the hydrogel (6-4-20), serial AFM images of the degradation areas were recorded, as shown in Figure 6C–N. From the dynamic optical bright field images (Figure 6C–F), we can clearly see that the network scaffold structures disappeared when meeting the water flow. AFM images of three areas on the hydrogel were acquired. Area i was the control area, which was not degraded, and the AFM image (Figure 6G) showed the thick network scaffold structures. Area ii was the peripheral area of the degraded hydrogel, and the AFM image (Figure 6H) showed that the thick scaffold structures became thin and began to melt (denoted by the arrow in Figure 6H). Besides, many particles were visible on the scaffold structures of hydrogel. Area iii was the central area of the degraded hydrogel, and the AFM image (Figure 6I) showed the compact network patches containing small pores, which were clearly visible from the higher resolution image (Figure 6J). A second drop of pure water was added to the degradation area for about 5 s. After pipetting the water out of the coverslip, AFM images were recorded (Figure 6K,L), clearly showing the discrete scaffold structures. Figure 6M,N shows the images of the degradation area after being washed by the third drop of water, and we can see that at this time scaffold structures disappeared and only nanoparticles (denoted by the circles in Figure 6M) were visible. The AFM imaging results (Figure 6) clearly revealed the dynamic morphological changes (thick scaffold structures → thin and compact network scaffold patches → discrete scaffold structures → discrete particles) during the degradation of the hydrogel, visually improving our understanding of the degradation of the Sundew-inspired hydrogel. The degradation of hydrogels was accompanied by the release of MG53 proteins. The three hydrogels (3-3-15, 6-4-20, and 7-8-27) used for drug release had different structural morphology and mechanical properties (Figure 4), which may reasonably result in the different degradations of the hydrogels and thus cause the different release of MG53 proteins encapsulated in the hydrogels.

Our previous studies have shown that the mucilage secreted by Sundew has a network nanofiber structure,[63] and the nanofiber is composed of nanoparticles.[64] Here, the AFM imaging results showed that the fabricated Sundew-inspired hydrogel exhibited a well-patterned network scaffold structure and nanoparticles were extensively distributed in the hydrogel (Figure 2M, Figure 4, and Figure S8). Gum arabic powder in water solution is a nanoparticle solution (Figure 5M,N), which serves as an important building block for constructing the Sundew-inspired hydrogel. The degradation of the fabricated Sundew-inspired hydrogel is the reverse process of the formation of the Sundew-inspired hydrogel, and we can clearly see that the final products of the degradation of the Sundew-inspired hydrogel were the nanoparticles (Figure 6M,N), indicating that nanoparticles were the fundamental elements for the fabricated Sundew-inspired hydrogels, which was similar to Sundew mucilage to some extent (the fundamental elements of Sundew mucilage are also

nanoparticles).[62,63] Alginate can form hydrogel in Ca^{2+}, and the cryo-SEM imaging results show that the alginate hydrogel has a network scaffold structure.[65] Here, we did not observe the network structures of alginate hydrogel via AFM imaging (Figure S6). This may be because alginate hydrogel is fragile, which makes it easily damaged by the AFM scanning tip due to the lateral forces caused by AFM tip. It is very difficult for AFM to visualize the morphology of alginate hydrogel, but SEM imaging that does not touch alginate hydrogel can easily visualize its detailed morphology. When there was gum arabic, alginate cross-linked with gum arabic particles via Ca^{2+} to form porous network scaffold structures (Figure 4). The introduction of gum arabic has greatly improved the strength of the scaffold structures, and AFM imaging clearly indicates the detailed morphology of the scaffold structures. Recently, researchers have paid great attention to utilizing double-network polymers[7,66] and nanoparticles[8,67] to fabricate the hydrogels with enhanced mechanical properties. Here, by introducing gum arabic particles to alginate polymer, adhesive hydrogels with tunable adhesion forces (Figure 3), structural scaffold, and mechanical properties (Figure 4) were developed, providing a novel way to fabricate sticky hydrogels based on natural biopolymers.

3.6. In Vivo Wound Healing and Toxicity Studies of the Sundew-Inspired Hydrogel

We first tested the potential toxicity and immunogenicity of Sundew-inspired hydrogel by subcutaneous administration into mice. For control, mice were injected with saline or commercial burn cream. This first-aid burn cream (Water-Jel Technologies, Carlstadt, NJ) was commercially available and frequently used to treat dermal wound caused by burn. Hence, we used it as a reference to examine the toxicity and immunogenicity of the Sundew-inspired hydrogel. Four weeks after injection, the injection sites were stained with F4/80 for detection of immune cell infiltration. As shown in Figure 7A, the samples derived from the Sundew-inspired hydrogel treatment group displayed minimal immune cell infiltration, indicating that Sundew hydrogel exhibit minimal immunogenicity. The percentage of F4/80 positive cell/total cell for the three groups was 316/2084 = 0.15 (saline), 409/2763 = 0.15 (burn cream), and 323/2664 = 0.12 (Sundew-inspired hydrogel), respectively. Thus, there were no significant differences between the three groups, indicating that the Sundew-inspired hydrogel did not produce adverse inflammation. In addition, major organs from experimental mice were collected and stained with H/E. As shown in Figure 7B, no abnormality was observed in major organs derived from the animals treated with Sundew-inspired hydrogel.

Next, to test the potential protective effects of Sundew-inspired hydrogel, we performed dermal wound healing experiments on wild mice. As summarized in Figure 8, the Sundew-inspired hydrogel exhibited enhanced capacity to promote in vivo wound healing with undetectable toxicity to major organs of treated mice. The mice were randomly grouped into four groups: saline group, rhMG53 group, Sundew-inspired hydrogel group, and Sundew-inspired hydrogel encapsulating rhMG53 group (Figure 8A). The hydrogel used for animal tests was chosen on the basis of its overall adhesion characteristics, mechanical properties, and morphological structures. Among the fabricated hydrogels (Figures 3 and 4), the hydrogel (6-4-20) had a relatively larger adhesion force (Figure 3), medium mechanical property, and compact network scaffold structure (Figure 4). Although the hydrogel (6-7-21)

had the largest adhesion force, its network scaffold structures were weaker than those of the hydrogel (6-4-20). Hence, we used the hydrogel (6-4-20) for in vivo animal tests. Upon excisional wounding, the wound sites were treated with one of the four treatments as mentioned above. The dosage of rhMG53 was 1 mg/kg for the mice. The healing process of each group then was photographed and quantified at different time points (Figure 8B). As shown in Figure 8C, the wound healing rate was significantly faster in Sundew hydrogel treatment as compared to saline treatment as control, suggesting that the Sundew-inspired hydrogel can facilitate wound healing. Figure 8D shows that, as compared to the saline group, wounds treated with rhMG53 displayed increased healing, and, more importantly, the combination of Sundew-inspired hydrogel and MG53 further improved the outcome of wound healing. The wounds almost totally closed 9 days after the treatment of Sundew-inspired hydrogel encapsulating rhMG53. MG53 protein has been shown to have therapeutic effects in promoting healing of wounds.[24] Here, we can see that, as compared to the treatment of rhMG53 alone, Sundew-inspired hydrogel encapsulation of rhMG53 further improves the therapeutic outcomes in wound healing.

To assess the quality of wound healing following the different treatment options, we performed pathology and histology analyses with the mice at 30 days post wound. Figure 9 shows the skin scar formation of the experimental mice treated by saline, rhMG53, Sundew-inspired hydrogel, or Sundew-inspired hydrogel encapsulating rhMG53 30 days after dermal wounding. Figure 9A showed the representative H&E and Masson's trichrome images of the skin tissues of mice treated by saline, rhMG53, Sundew-inspired hydrogel, or Sundew-inspired hydrogel encapsulating rhMG53 at 30 days after dermal wounding. Figure 9B is the quantification of skin thickness from the four groups. As compared to the control group (treated by saline), the group treated with Sundew-inspired hydrogel had similar thickness, representing a similar degree of scarring. Thus, treatment with the Sundew-inspired hydrogel could promote the healing process but could not impact fibrosis. Consistent with our previous studies with rhMG53 in suppression of fibrosis associated with chronic wound healing,[25] mice treated with rhMG53 showed reduced skin thickness as compared to control ($p < 0.01$) indicative of reduced fibrosis remodeling. Moreover, mice treated with Sundew-inspired hydrogel encapsulated with rhMG53 also show reduced skin thickness (Figure 9B). Collectively, the in vivo results showed the potential role of Sundew-inspired hydrogel in wound healing, whether used alone or as a rhMG53 delivery system for promoting wound healing and suppressing scarring.

Currently, in the field of drug development, protein drugs have gained a significant role in almost every field of medicine, and encapsulating proteins with hydrogels has attracted the great attention of researchers.[62,68] Hydrogels have cross-linked networks of polymers and are capable of retaining large amounts of water, which is useful for keeping proteins in their active form and preventing them from denaturation.[69] Especially adhesive hydrogels are advantageous in certain fields, such as surgical sealant, cell adhesion, and tissue regeneration. Fibrin glues are widely used as biological tissue adhesives in surgical practices, but their mechanical property is not sufficient, whereas cyanoacrylate-based synthetic adhesive glues can solidify upon contact with tissues, but acrylic derivatives are toxic.[70] Here, bioinspired sticky hydrogels with tunable adhesion, structural, and mechanical

properties were developed to deliver therapeutic proteins to promote wound healing, providing novel possibilities in the field of protein delivery by bioadhesives.

4. CONCLUSIONS

This work has demonstrated the use of natural biopolymers consisting of alginate and gum arabic to fabricate a Sundew-inspired sticky hydrogel, which has notable potential in sustained drug delivery and chronic wound healing applications. Orthogonal experimental design was used to obtain hydrogels with enhanced adhesion characteristics and tunable properties for quick and sustained drug delivery. AFM and rheological measurements showed that the Sundew-inspired hydrogels maintained micro-/nanostructures (micro scaffolds, nanoparticles) with adhesion characteristics and mechanical properties appropriate for the encapsulation of rhMG53 protein. rhMG53 protein was encapsulated in the hydrogels by binding to the gum arabic particles via electrostatic adsorption, and the morphological changes during hydrogel degradation provide a mechanism for sustained delivery of the rhMG53 through topical administration. In vitro drug release and in vivo animal studies demonstrated the efficiency of the Sundew-inspired hydrogels in drug delivery and chronic wound healing. Taken together, this study provides a method to develop and investigate bioinspired hydrogels from micro-/nanoscale morphology and adhesion characteristics of Sundew plant to macro mechanical properties integrated with molecular mechanisms, which enable a novel biomaterial environment to support cell proliferation and therapeutic applications.

Supplementary Material

Refer to Web version on PubMed Central for supplementary material.

Acknowledgments

References

1. Li J, Mooney DJ. Designing Hydrogels for Controlled Drug Delivery. Nat. Rev. Mater. 2016; 1(12): 16071. [PubMed: 29657852]

2. Seliktar D. Designing Cell-Compatible Hydrogels for Biomedical Applications. Science. 2012; 336(6085):1124–1128. [PubMed: 22654050]

3. Hoffman AS. Hydrogels for Biomedical Applications. Adv. Drug Delivery Rev. 2012; 64:18–23.

4. Lee KY, Mooney DJ. Alginate: Properties and Biomedical Applications. Prog. Polym. Sci. 2012; 37(1):106–126. [PubMed: 22125349]

5. Gombotz WR, Wee SF. Protein Release from Alginate Matrices. Adv. Drug Delivery Rev. 2012; 64:194–205.

6. Desai RM, Koshy ST, Hilderbrand SA, Mooney DJ, Joshi NS. Versatile Click Alginate Hydrogels Crosslinked via Tetrazine-Norbornene Chemistry. Biomaterials. 2015; 50:30–37. [PubMed: 25736493]

7. Sun JY, Zhao X, Illeperuma WRK, Chaudhuri O, Oh KH, Mooney DJ, Vlassak JJ, Suo Z. Highly Stretchable and Tough Hydrogels. Nature. 2012; 489(7414):133–136. [PubMed: 22955625]

8. Rose S, Prevoteau A, Elziere P, Hourdet D, Marcellan A, Leibler L. Nanoparticle Solutions as Adhesives for Gels and Biological Tissues. Nature. 2014; 505(7483):382–385. [PubMed: 24336207]

9. Li Q, Barrett DG, Messersmith PB, Holten-Anderson N. Controlling Hydrogel Mechanics via Bio-inspired Polymer-Nanoparticle Bond Dynamics. ACS Nano. 2016; 10(1):1317–1324. [PubMed: 26645284]

10. Caliari SR, Burdick JA. A Practical Guide to Hydrogels for Cell Culture. Nat. Methods. 2016; 13(5):405–414. [PubMed: 27123816]

11. Peak CW, Wilker JJ, Schmidt G. A Review on Tough and Sticky Hydrogels. Colloid Polym. Sci. 2013; 291(9):2031–2047.

12. Lee H, Lee BP, Messersmith PB. A Reversible Wet/Dry Adhesive Inspired by Mussels and Geckos. Nature. 2007; 448(7151):338–341. [PubMed: 17637666]

13. Zhang M, Liu M, Prest H, Fischer S. Nanoparticles Secreted from Ivy Rootlets for Surface Climbing. Nano Lett. 2008; 8(5):1277–1280. [PubMed: 18355053]

14. Kwak MK, Pang C, Jeong HE, Kim HN, Yoon H, Jung HS, Suh KY. Towards the Next Level of Bioinspired Dry Adhesives: New Designs and Applications. Adv. Funct. Mater. 2011; 21(19): 3606–3616.

15. Oh DX, Kim S, Lee D, Hwang DS. Tunicate-Mimetic Nanofibrous Hydrogel Adhesive with Improved Wet Adhesion. Acta Biomater. 2015; 20:104–112. [PubMed: 25841348]

16. Yang SY, Cearbhaill ED, Sisk GC, Park KM, Cho WK, Villiger M, Bouma BE, Pomahac B, Karp JM. A Bio-inspired Wwellable Microneedle Adhesive for Mechanical Interlocking with Tissue. Nat. Commun. 2013; 4:1702. [PubMed: 23591869]

17. Heinzmann C, Weder C, Espinosa LM. Supramolecular Polymer Adhesives: Advanced Materials Inspired by Nature. Chem. Soc. Rev. 2016; 45(2):342–358. [PubMed: 26203784]

18. Green JJ, Elisseeff JH. Mimicking Biological Functionality with Polymers for Biomedical Applications. Nature. 2016; 540(7633):386–394. [PubMed: 27974772]

19. Nakamura Y, Reichelt M, Mayer VE, Mithofer A. Jasmonates Trigger Prey-Induced Formation of 'Outer Stomach' in Carnivorous Sundew Plants. Proc. R. Soc. London, Ser. B. 2013; 280(1759): 20130228.

20. Adlassnig, W., Lendl, T., Peroutka, M., Lang, I. Deadly Glue -Adhesive Traps of Carnivorous Plants. In: von Byern, J., Grunwald, I., editors. Biological Adhesive Systems. Springer; New York: 2010. p. 15-28.

21. Phillips AO, Phillips GO. Biofunctional Behaviour and Health Benefits of a Specific Gum Arabic. Food Hydrocolloids. 2011; 25(2):165–169.

22. Prajapati VD, Jani GK, Moradiya NG, Randeria NP. Pharmaceutical Applications of Various Natural Gums, Mucilages and Their Modified Forms. Carbohydr. Polym. 2013; 92(2):1685–1699. [PubMed: 23399207]

23. Li M, Liu L, Xi N, Wang Y, Xiao X, Zhang W. Nanoscale Imaging and Mechanical Analysis of Fc Receptor-Mediated Macrophage Phagocytosis against Cancer Cells. Langmuir. 2014; 30(6):1609–1621. [PubMed: 24495237]

24. Cai C, Masumiya H, Weisleder N, Matsuda N, Nishi M, Hwang M, Ko JK, Lin P, Thornton A, Zhao X, Pan Z, Komazaki S, Brotto M, Takeshima H, Ma J. MG53 Nucleates Assembly of Cell Membrane Repair Machinery. Nat. Cell Biol. 2009; 11(1):56–64. [PubMed: 19043407]

25. Li H, Duann P, Lin P, Zhao L, Fan Z, Tan T, Zhou X, Sun M, Fu M, Orange M, Sermersheim M, Ma H, He D, Steinberg SM, Higgins R, Zhu H, John E, Zeng C, Guan J, Ma J. Modulation of Wound Healing and Scar Formation by MG53 Protein-Mediated Cell Membrane Repair. J. Biol. Chem. 2015; 290(40):24592–24603. [PubMed: 26306047]

26. Duan P, Li H, Lin P, Tan T, Wang Z, Chen K, Zhou X, Gumpper K, Zhu H, Ludwig T, Mohler PJ, Rovin B, Abraham WT, Zeng C, Ma J. MG53-Mediated Cell Membrane Repair Protects against Acute Kidney Injury. Sci. Transl. Med. 2015; 7(279):279ra36.

27. Poppinga S, Masselter T, Speck T. Faster than Their Prey: New Insights into the Rapid Movements of Active Carnivorous Plants Traps. BioEssays. 2013; 35(7):649–657. [PubMed: 23613360]

28. Sun L, Huang Y, Bian Z, Petrosino J, Fan Z, Wang Y, Park KH, Yue T, Schmidt M, Galster S, Ma J, Zhu H, Zhang M. Sundew-Inspired Adhesive Hydrogels Combined with Adipose-Derived Stem Cells for Wound Healing. ACS Appl. Mater. Interfaces. 2016; 8(3):2423–2434. [PubMed: 26731614]

29. Wang Q, Burchard W, Cui SW, Huang X, Phillips GO. Solution Properties of Conventional Gum Arabic and A Matured Gum Arabic (Acacia (Sen) Super Gum). Biomacromolecules. 2008; 9(4): 1163–1169. [PubMed: 18324777]

30. Li M, Xiao X, Liu L, Xi N, Wang Y. Rapid Recognition and Functional Analysis of Membrane Proteins on Human Cancer Cells Using Atomic Force Microscopy. J. Immunol. Methods. 2016; 436:41–49. [PubMed: 27374866]

31. Geim AK, Dubonos SV, Grigorieva IV, Novoselov KS, Zhukov AA, Shapoval SY. Microfabricated Adhesive Mimicking Gecko Foot-Hair. Nat. Mater. 2003; 2(7):461–463. [PubMed: 12776092]

32. Pussak D, Ponader D, Mosca S, Pompoe T, Hartmann L, Schmidt S. Specific Adhesion of Carbohydrate Hydrogel Particles in Competition with Multivalent Inhibitors Evaluated by AFM. Langmuir. 2014; 30(21):6142–6150. [PubMed: 24806833]

33. Helfricht N, Doblhofer E, Bieber V, Lommes P, Sieber V, Scheibel T, Papastavrou G. Probing the Adhesion Properties of Alginate Hydrogels: a New Approach Towards the Preparation of Soft Colloidal Probes for Direct Force Measurements. Soft Matter. 2017; 13(3):578–589. [PubMed: 27976776]

34. Ghobril C, Grinstaff MW. The Chemistry and Engineering of Polymeric Hydrogel Adhesives for Wound Closure: a Tutorial. Chem. Soc. Rev. 2015; 44(7):1820–1835. [PubMed: 25649260]

35. Choi YC, Choi JS, Jung YJ, Cho YW. Human Gelatin Tissue-Adhesive Hydrogels Prepared by Enzyme-Mediated Biosynthesis of DOPA and Fe^{3+} Ion Crosslinking. J. Mater. Chem. B. 2014; 2(2):201–209.

36. Sun J, Wei D, Zhu Y, Zhong M, Zuo Y, Fan H, Zhang X. A Spatial Patternable Macroporous Hydrogel with Cell-Affinity Domains to Enhance Cell Spreading and Differentiation. Biomaterials. 2014; 35(17):4759–4768. [PubMed: 24636216]

37. Balakrishnan B, Joshi N, Jayakrishnan A, Banerjee R. Self-Crosslinked Oxidized Alginate/Gelatin Hydrogel as Injectable, Adhesive Biomimetic Scaffolds for Cartilage Regeneration. Acta Biomater. 2014; 10(8):3650–3663. [PubMed: 24811827]

38. Lutolf MP, Gilbert PM, Blau HM. Designing Materials to Direct Stem-Cell Fate. Nature. 2009; 462(7272):433–441. [PubMed: 19940913]

39. Pan L, Yu G, Zhai D, Lee HR, Zhao W, Liu N, Wang H, Tee BCK, Shi Y, Cui Y, Bao Z. Hierarchical Nanostructured Conducting Polymer Hydrogel with High Electrochemical Activity. Proc. Natl. Acad. Sci. U. S. A. 2012; 109(24):9287–9292. [PubMed: 22645374]

40. Zhang H, Patel A, Gaharwar AK, Mihaila SM, Iviglia G, Mukundan S, Bae H, Yang H, Khademhosseini A. Hyperbranched Polyester Hydrogels with Controlled Drug Release and Cell Adhesion Properties. Biomacromolecules. 2013; 14(5):1299–1310. [PubMed: 23394067]

41. Koutsopoulos S, Zhang S. Two-Layered Injectable Self-Assembling Peptide Scaffold Hydrogels for Long-Term Sustained Release of Human Antibodies. J. Controlled Release. 2012; 160(3):451–458.

42. Jaggy M, Zhang P, Greiner AM, Autenrieth TJ, Nedashkivska V, Efremov AN, Blattner C, Bastmeyer M, Levkin PA. Hierarchical Micro-Nano Surface Topography Promotes Long-Term Maintenance of Undifferentiated Mouse Embryonic Stem Cells. Nano Lett. 2015; 15(10):7146–7154. [PubMed: 26351257]

43. Raeburn J, Zamith Cardoso A, Adams DJ. The Importance of the Self-Assembly Process to Control Mechanical Properties of Low Molecular Weight Hydrogels. Chem. Soc. Rev. 2013; 42(12):5143–5156. [PubMed: 23571407]

44. Kai D, Prabhakaran MP, Stahl B, Eblenkamp M, Wintermantel E, Ramakrishna S. Mechanical Properties and in Vitro Behavior of Nanofiber-Hydrogel Composites for Tissue Engineering Applications. Nanotechnology. 2012; 23(9):095705. [PubMed: 22322583]

45. Cao B, Tang Q, Li L, Humble J, Wu H, Liu L, Cheng G. Switchable Antimicrobial and Antifouling Hydrogels with Enhanced Mechanical Properties. Adv. Healthcare Mater. 2013; 2(8):1096–1102.

46. Higuchi A, Ling QD, Chang Y, Hsu ST, Umezawa A. Physical Cues of Biomaterials Guide Stem Cell Differentiation Fate. Chem. Rev. 2013; 113(5):3297–3328. [PubMed: 23391258]

47. Trappmann B, Chen CS. How Cells Sense Extracellular Matrix Stiffness: a Material's Perspective. Curr. Opin. Biotechnol. 2013; 24(5):948–953. [PubMed: 23611564]

48. Garcia JR, Garcia AJ. Cellular Mechanotransduction: Sensing Rigidity. Nat. Mater. 2014; 13(6): 539–540. [PubMed: 24845988]

49. Nagelkerke A, Bussink J, Rowan AE, Span PN. The Mechanical Microenvironment in Cancer: How Physics Affects Tumours. Semin. Cancer Biol. 2015; 35:62–70. [PubMed: 26343578]

50. Draeger A, Schoenauer R, Atanassoff AP, Wolfmeier H, Babiychuk EB. Dealing with Damage: Plasma Membrane Repair Mechanisms. Biochimie. 2014; 107:66–72. [PubMed: 25183513]

51. Cooper ST, McNeil PL. Membrane Repair: Mechanisms and Pathophysiology. Physiol. Rev. 2015; 95(4):1205–1240. [PubMed: 26336031]

52. Yao Y, Zhang B, Zhu H, Li H, Han Y, Chen K, Wang Z, Zeng J, Liu Y, Wang X, Li Y, He D, Lin P, Zhou X, Park KH, Bian Z, Chen Z, Gong N, Tan T, Zhou J, Zhang M, Ma J, Zeng C. MG53 Permeates through Blood-Brain Barrier to Protect Ischemic Brain Injury. Oncotarget. 2016; 7:22474–22485. [PubMed: 26967557]

53. He B, Tang RH, Weisleder N, Xiao B, Yuan Z, Cai C, Zhu H, Lin P, Qiao C, Li J, Mayer C, Li J, Ma J, Xiao X. Enhancing Muscle Membrane Repair by Gene Delivery of MG53 Ameliorates Muscular Dystrophy and Heart Failure in δ-Sarcoglycan-Deficient Hamsters. Mol. Ther. 2012; 20(4):727–735. [PubMed: 22314291]

54. Weisleder N, Takizawa N, Lin P, Wang X, Cao C, Zhang Y, Tan T, Ferrante C, Zhu H, Chen PJ, Yan R, Sterling M, Zhao X, Hwang M, Takeshima M, Cai C, Cheng H, Takeshima H, Xiao RP, Ma J. Recombinant MG53 Protein Modulates Therapeutic Cell Membrane Repair in Treatment of Muscular Dystrophy. Sci. Transl. Med. 2012; 4(139) 139ra85-1.

55. Jia Y, Chen K, Lin P, Lieber G, Nishi M, Yan R, Wang Z, Yao Y, Li Y, Whitson BA, Duan P, Li H, Zhou X, Zhu H, Takeshima H, Hunter JC, McLeod RL, Weisleder N, Zeng C, Ma J. Treatment of Acute Lung Injury by Targeting MG53-Mediated Cell Membrane Repair. Nat. Commun. 2014; 5:4387. [PubMed: 25034454]

56. Zhu H, Hou J, Roe JL, Park KH, Tan T, Zheng Y, Li L, Zhang C, Liu J, Liu Z, Ma J, Walters TJ. Amelioration of Ischemia-Reperfusion-Induced Muscle Injury by the Recombinant Human MG53 Protein. Muscle Nerve. 2015; 52(5):852–858. [PubMed: 25703692]

57. Liu J, Zhu H, Zheng Y, Xu Z, Li L, Tan T, Park KH, Hou J, Zhang C, Li D, Li R, Liu Z, Weisleder N, Zhu D, Lin P, Ma J. Cardioprotection of Recombinant Human MG53 Protein in a Porcine Model of Ischemia and Reperfusion Injury. J. Mol. Cell. Cardiol. 2015; 80:10–19. [PubMed: 25533937]

58. Ngouemazong ED, Christiaens S, Shpigelman A, Van Loey A, Hendrickx M. The Emulsifying and Emulsion-Stabilizing Properties of Pectin: a Review. Compr. Rev. Food Sci. Food Saf. 2015; 14(6):705–718.

59. Bouyer E, Mekhloufi G, Huang N, Rosilio V, Agnely F. β-lactoglobulin, Gum Arabic, and Xanthan Gum for Emulsifying Sweet Almond Oil: Formulation and Stabilization Mechanisms of Pharmaceutical Emulsions. Colloids Surf., A. 2013; 433:77–87.

60. Moschakis T, Murray BS, Biliaderis CG. Modifications in Stability and Structure of Whey Protein-Coated O/W Emulsions by Interacting Chitosan and Gum Arabic Mixed Dispersions. Food Hydrocolloids. 2010; 24(1):8–17.

61. Censi R, Di Martino P, Vermonden T, Hennink WE. Hydrogels for Protein Delivery in Tissue Engineering. J. Controlled Release. 2012; 161(2):680–692.

62. Vermonden T, Censi R, Hennink WE. Hydrogels for Protein Delivery. Chem. Rev. 2012; 112(5): 2853–2888. [PubMed: 22360637]

63. Zhang M, Lenaghan SC, Xia L, Dong L, He W, Henson WR, Fan X. Nanofibers and Nanoparticles from the Insect-Capturing Adhesive of the Sundew (Drosera) for Cell Attachment. J. Nanobiotechnol. 2010; 8:20.

64. Huang Y, Wang Y, Sun L, Agrawal R, Zhang M. Sundew Adhesive: a Naturally Occurring Hydrogel. J. R. Soc., Interface. 2015; 12(107):20150226. [PubMed: 25948615]

65. Jejurikar A, Lawrie G, Martin D, Grondahl L. A Novel Strategy for Preparing Mechanically Robust Ionically Cross-Linked Alginate Hydrogels. Biomed. Mater. 2011; 6(2):025010. [PubMed: 21436510]

66. Cong HP, Wang P, Yu SH. Stretchable and Self-Healing Graphene Oxide-Polymer Composite Hydrogels: a Dual-Network Design. Chem. Mater. 2013; 25(16):3357–3362.

67. Appel EA, Tibbitt MW, Webber MJ, Mattix BA, Veiseh O, Langer R. Self-Assembled Hydrogels Utilizing Polymer-Nanoparticle Interactions. Nat. Commun. 2015; 6:6295. [PubMed: 25695516]

68. Tibbitt MW, Dahlman JE, Langer R. Emerging Frontiers in Drug Delivery. J. Am. Chem. Soc. 2016; 138(3):704–717. [PubMed: 26741786]

69. Bae KH, Kurisawa M. Emerging Hydrogel Designs for Controlled Protein Delivery. Biomater. Sci. 2016; 4(8):1184–1192. [PubMed: 27374633]

70. Lih E, Lee JS, Park KM, Park KD. Rapidly Curable Chitosan-PEG Hydrogels as Tissue Adhesives for Hemostasis and Wound Healing. Acta Biomater. 2012; 8(9):3261–3269. [PubMed: 22617740]
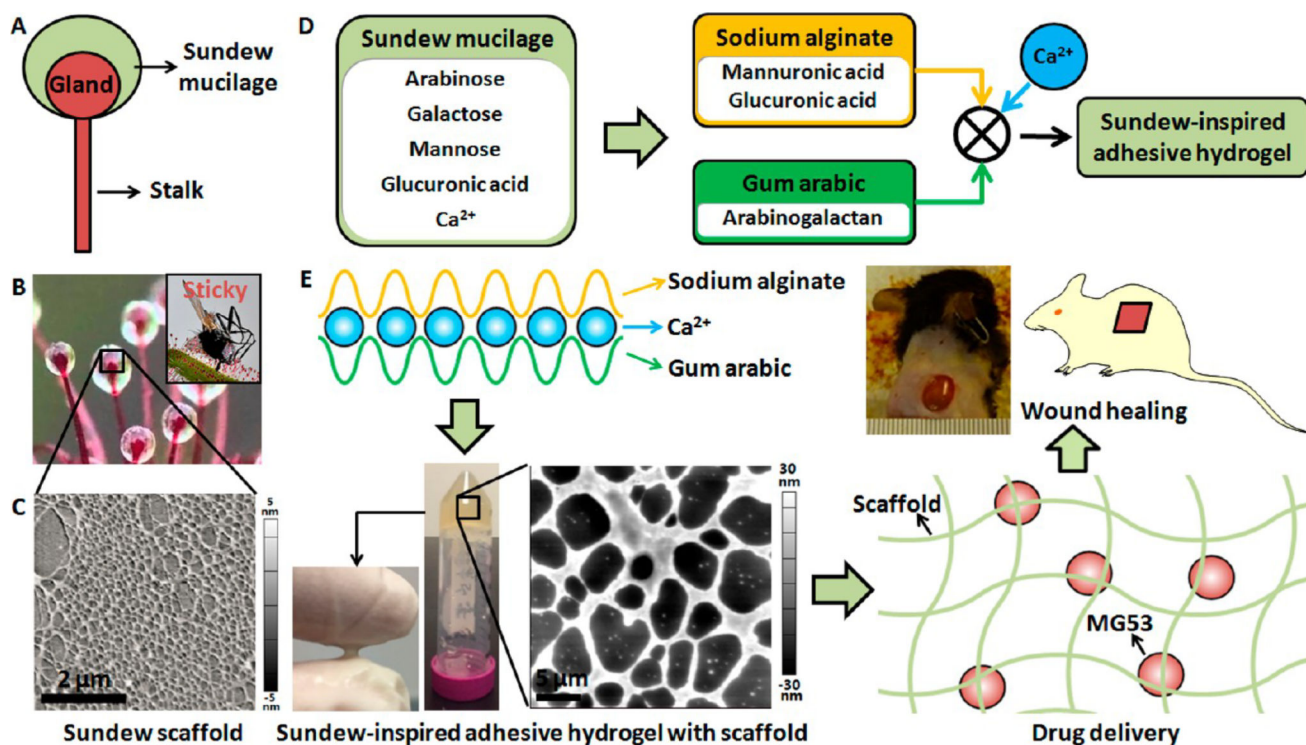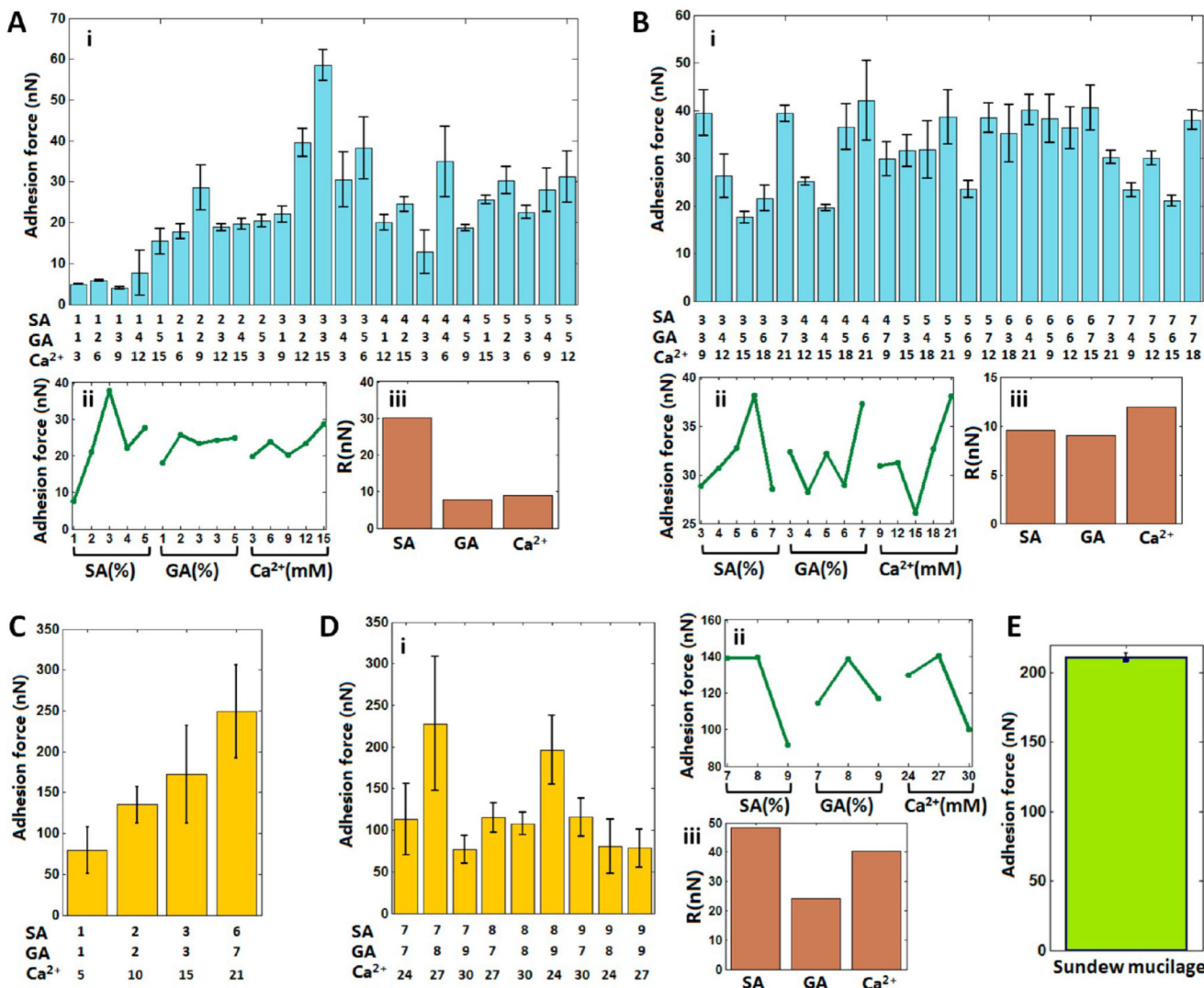
Figure 1.
Sundew-inspired adhesive hydrogel for controlled drug delivery in chronic wound healing.
(A,B) Schematic diagram (A) and actual image (B) of the Sundew mucilage. Inset in (B)
shows a prey trapped by the Sundew mucilage. (C) AFM topographic micrograph of the
Sundew mucilage. (D) Sodium alginate, gum arabic, and Ca^{2+} are used to fabricate the
Sundew-inspired adhesive hydrogel. (E) Hydrogels are formed by Ca^{2+}-dependent cross-
linking between sodium alginate and gum arabic. After dropping the fabricated Sundew-
inspired hydrogel onto a finger, the adhesion characteristics of the hydrogel were sensed by
touching and pulling the hydrogel with another finger. AFM topographic micrograph shows
network porous scaffold structures of the fabricated Sundew-inspired hydrogel. The
Sundew-inspired hydrogel was used for drug delivery and chronic wound healing to explore
its potential biomedical applications.
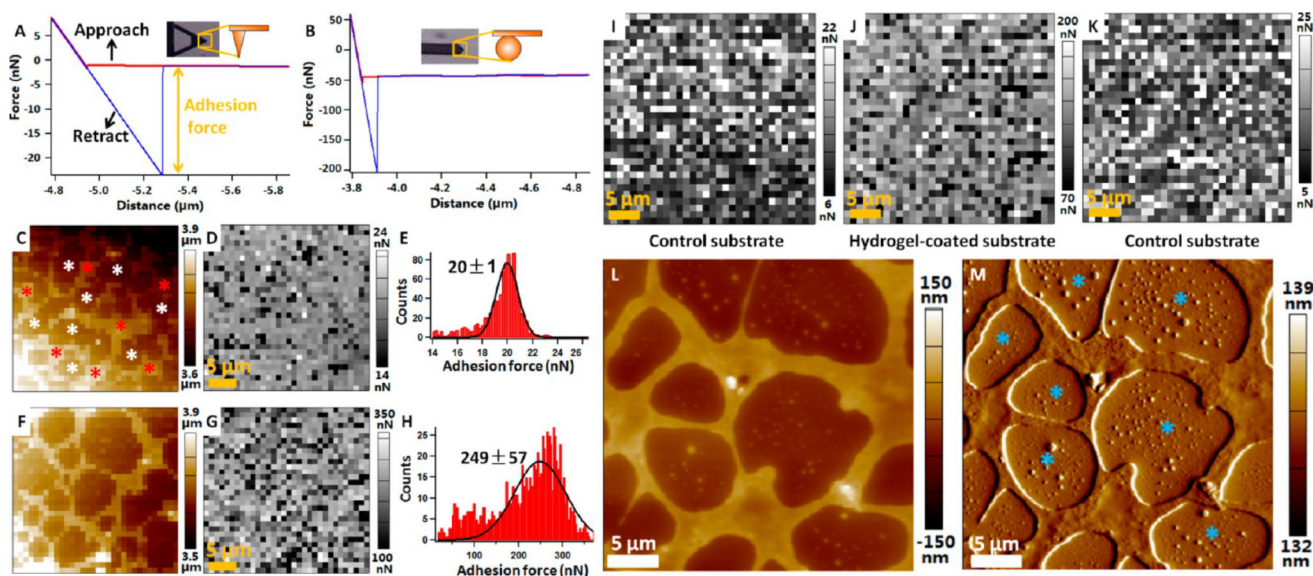
Figure 2.

Quantification of the adhesion characteristics of the fabricated Sundew-inspired hydrogels by AFM force spectroscopy. (A,B) Representative force curves recorded on the hydrogel-coated glass substrate with conical tip (A) and spherical tip (B). The red curve corresponds to the approach process, and the blue curve corresponds to the retract process. Adhesion force is calculated from the retract curve and is equal to the magnitude of the peak. The insets are the optical images and schematic diagrams of tips. (C,D) Topography image (C) and adhesion force map (D) recorded at the force volume mode by conical tip. During force volume mode, 32×32 force curves were obtained in 35×35 μm^2 areas of the hydrogel-coated glass substrate. The red asterisks indicate network porous scaffold area, and the white asterisks indicate the blank area. (E) Histogram and Gaussian fitting of the adhesion forces in (D). (F,G) Topography image (F) and adhesion force (G) recorded on 35×35 μm^2 areas of the hydrogel-coated glass substrate by spherical tip. (H) Histogram and Gaussian fitting of the adhesion forces in (G). (I–K) Adhesion forces measured on control substrate (without hydrogel) and hydrogel-coated substrate by spherical tip. Adhesion measurements were performed on control substrate first (I), and then adhesion measurements were performed on hydrogel-coated substrate (J) with the same AFM tip. Finally, the same AFM tip was used to measure the adhesion force on control substrate again (K). (L,M) AFM height image (L) and deflection image (M) of the hydrogel-coated substrate. The blue asterisks indicate nanoparticles in the blank area of the hydrogel.
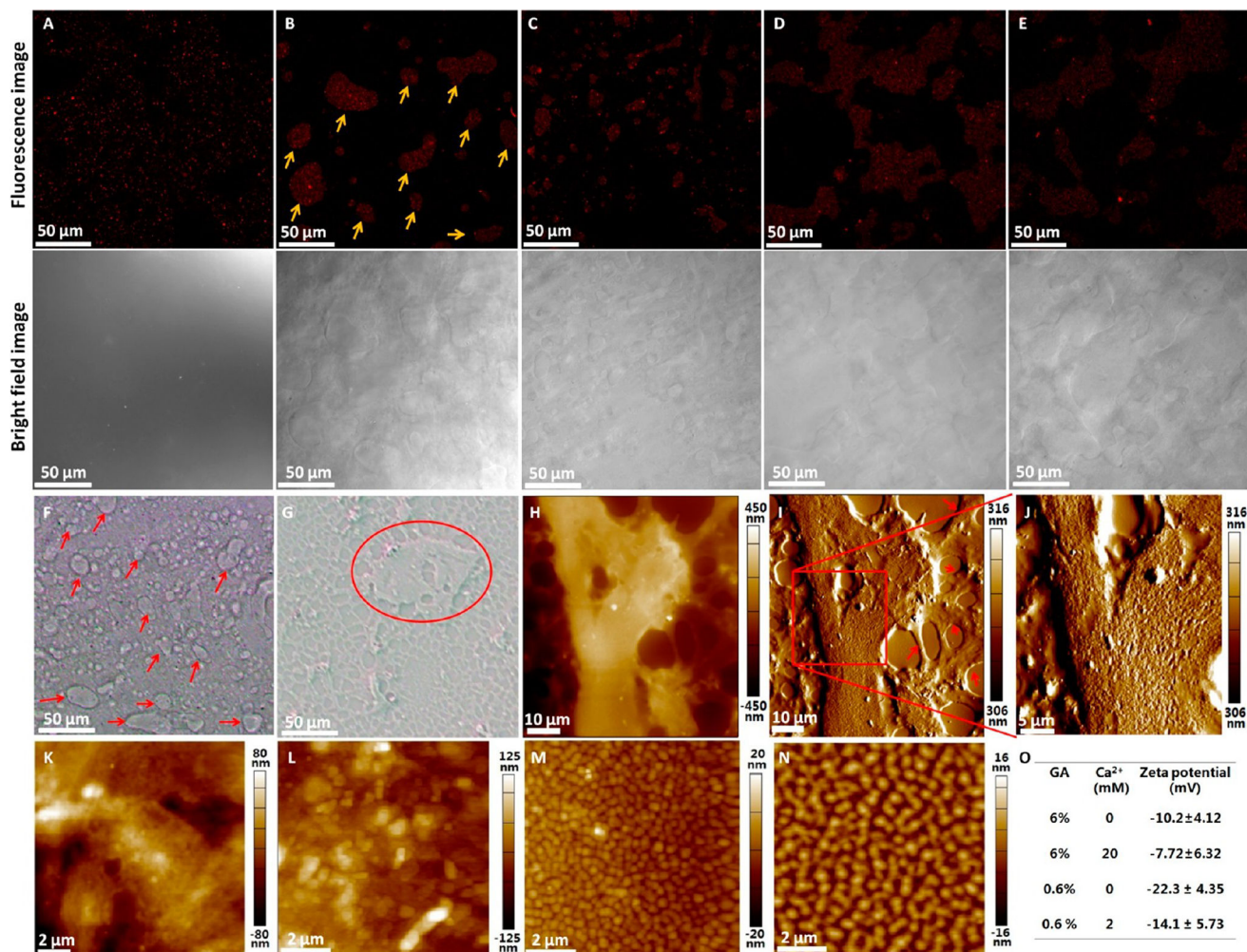
Figure 3.
Adhesion forces of the Sundew-inspired hydrogels with different component ratios via orthogonal experimental design. (A,B) Adhesion forces of hydrogels measured by a conical tip in $L_{25}(5^3)$ orthogonal experiments. (C,D) Adhesion forces of hydrogels measured by a spherical tip. (C) Adhesion forces of four hydrogels. (D) Adhesion forces of the hydrogels in $L_9(3^3)$ orthogonal experiments. (i) Histograms of adhesion forces in orthogonal experiments. (ii) Average adhesion forces for the different levels of each component in orthogonal experiments. (iii) Importance factors of each component in the orthogonal experiments. Importance factors indicate the importance of the three components in determining the adhesion force of the hydrogels. (E) Adhesion forces of the mucilage secreted by Sundew.
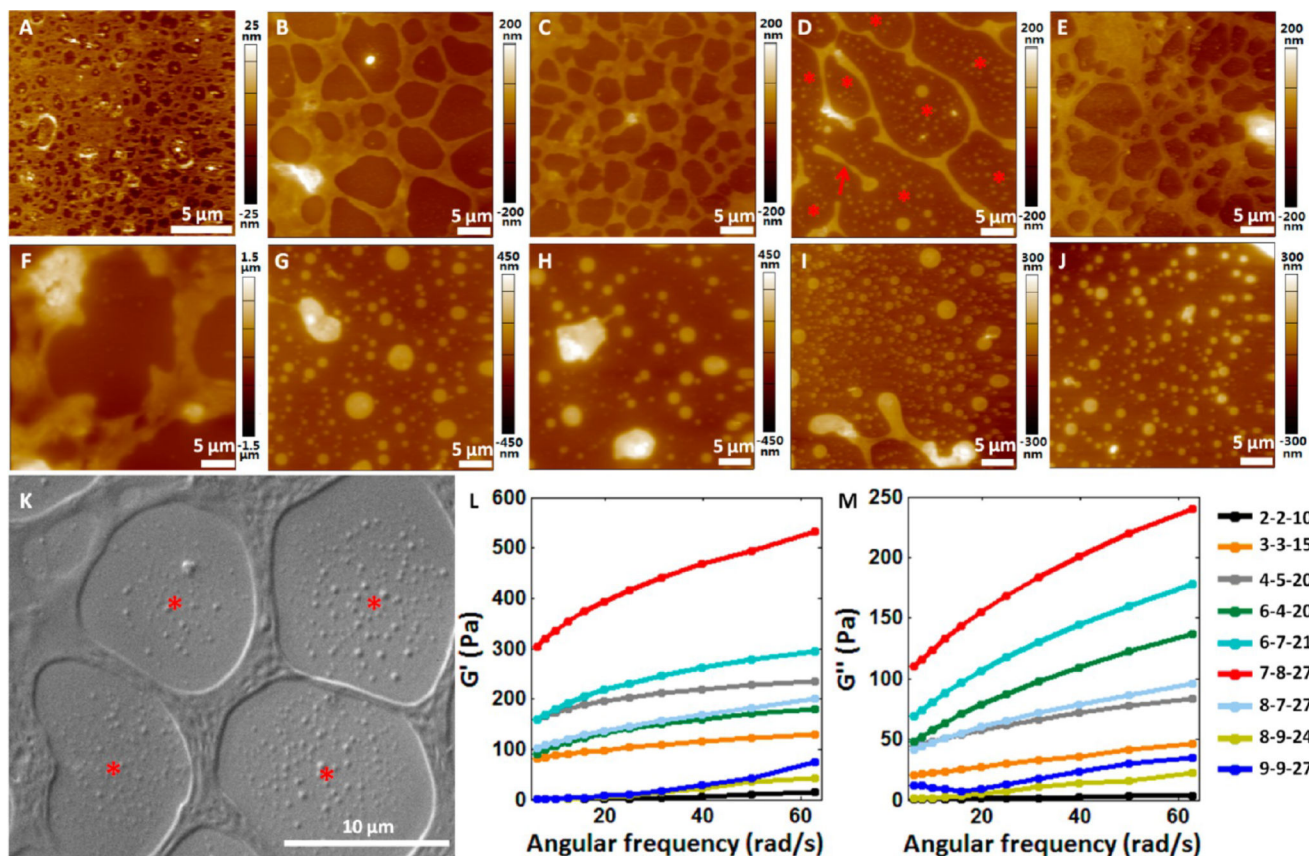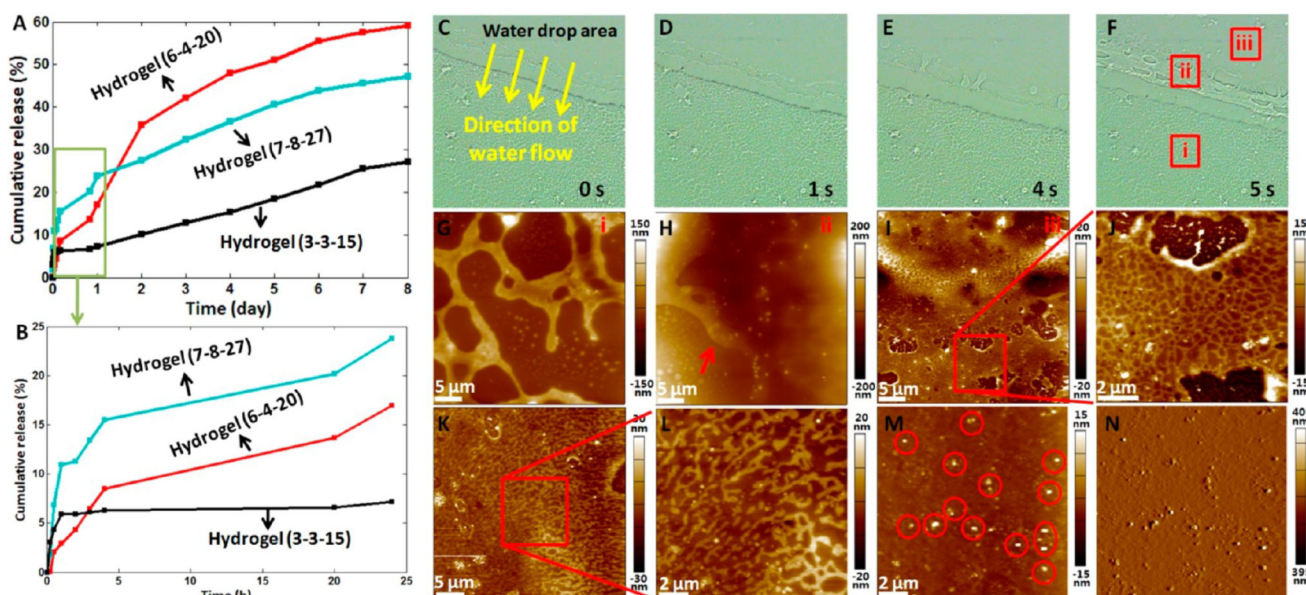
Figure 4.
Structural and mechanical properties of the hydrogels with different component (sodium alginate, gum arabic, Ca^{2+}) ratios. (A–J) AFM height images of the hydrogels with different component ratios. (A) Hydrogel (1-1-5). (B) Hydrogel (2-2-10). (C) Hydrogel (3-3-15). (D) Hydrogel (4-5-20). The red arrow indicates the discretely distributed scaffold. The red asterisks indicate the nanoparticles distributed in the non scaffold areas. (E) Hydrogel (6-4-20). (F) Hydrogel (6-7-21). (G) Hydrogel (7-8-27). (H) Hydrogel (8-7-27). (I) Hydrogel (8-9-24). (J) Hydrogel (9-9-27). (K) SEM image of the hydrogel (3-3-15). The red asterisks indicate the nanoparticles distributed in the non scaffold areas. (L,M) Mechanical properties of the nine hydrogels with different component ratios measured by rheometer. (L) Storage modulus (G') of the hydrogels. (M) Loss modulus (G'') of the hydrogels.
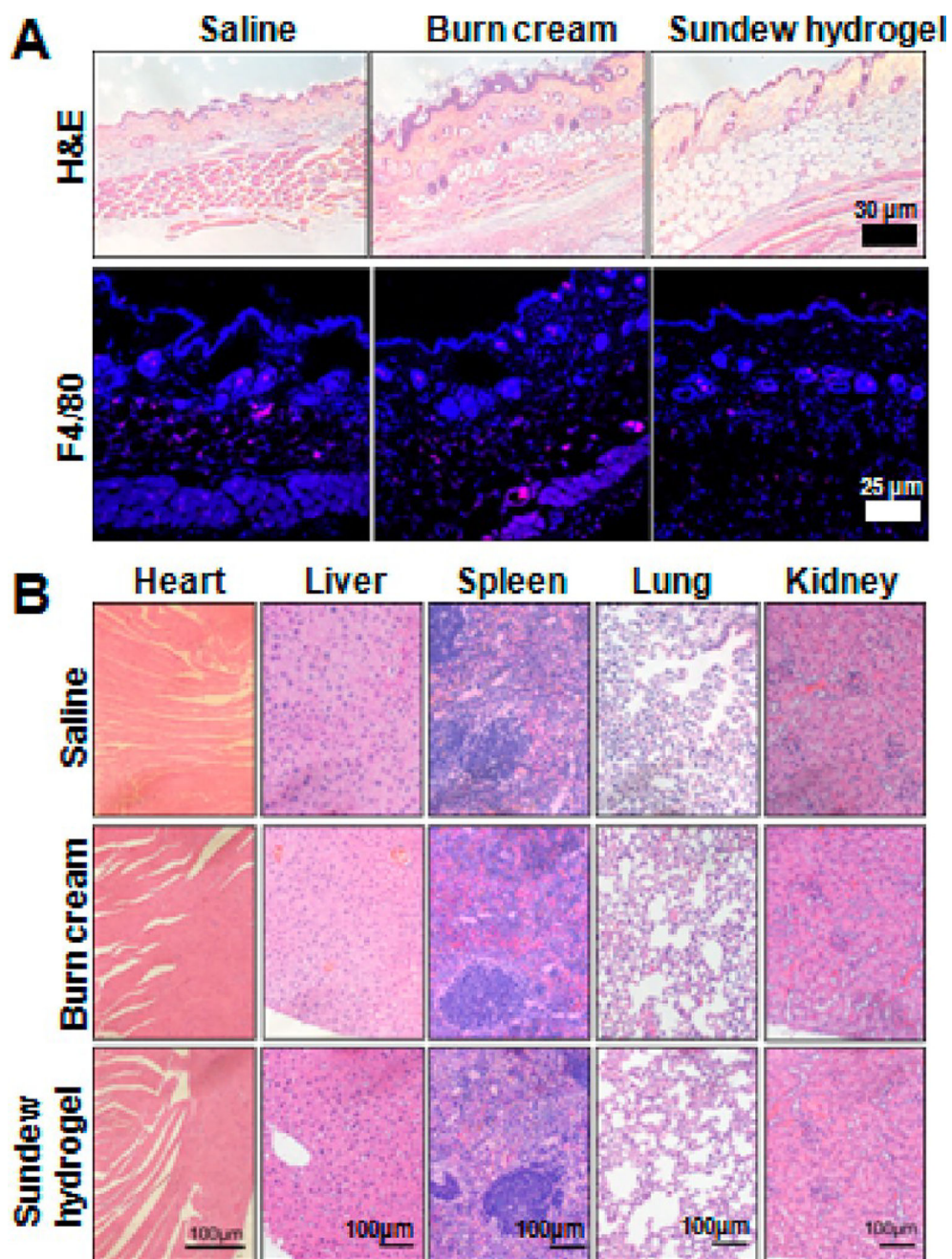
Figure 5.
Encapsulation of rhMG53 by Sundew-inspired hydrogels. (A–E) Confocal fluorescence microscopy of Alexa 647-labeled MG53s packed in different hydrogels. For each hydrogel, one typical fluorescence image and one corresponding optical bright field image were shown. (A) Hydrogel (3-3-15). (B) Hydrogel (4-5-20). The red arrows in (B) indicate the localized reservoir area containing MG53. (C) Hydrogel (6-4-20). (D) Hydrogel (6-7-21). (E) Hydrogel (8-7-27). (F–O) Exploring the mechanisms of interactions between MG53 proteins and Sundew-inspired hydrogels. (F,G) Optical bright images of MG53-packed hydrogel (6-4-20). (F) was obtained by pipetting a drop of hydrogel onto a coverslip, and (G) was obtained by scratching the hydrogel drop with another coverslip to form a thin layer on the coverslip. Reservoir areas are denoted by the arrows in (F) and circle in (G). (H–J) AFM height image (H), AFM deflection image (I), and higher resolution AFM deflection image (J) of a reservoir area of the hydrogel. The red arrows in (I) indicate the scaffolds. (K) AFM height image of the reservoir area of the hydrogel (6-4-20). (L) AFM height image of the reservoir area of the hydrogel (6-6-20). (M) AFM height image of the solution (0-6-20). (N) AFM height image of the solution (0-8-20). (O) Zeta potential gum arabic nanoparticles in pure water.
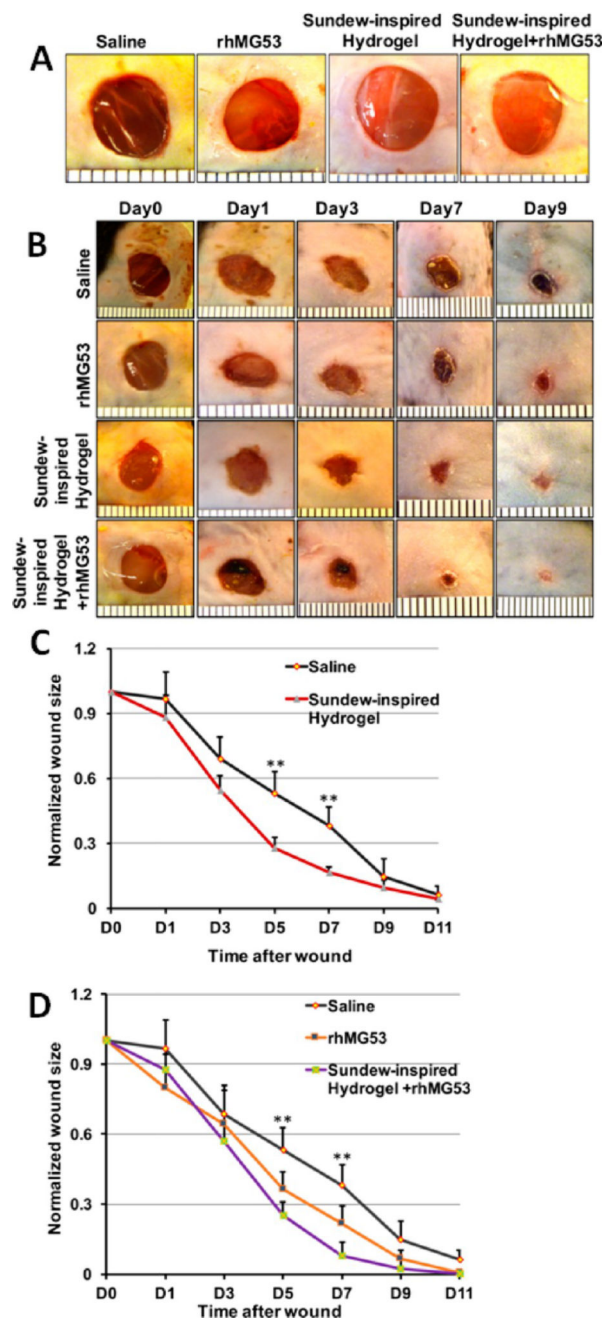
Figure 6.
In vitro drug release and hydrogel degradation. (A,B) In vitro release of MG53 in three types of hydrogels. (A) Release in 8 days. (B) Release in 24 h. (C–N) Morphological changes of the hydrogel (6-4-20) during degradation in vitro. (C–F) Successive optical bright field images of the hydrogel coated on a coverslip after pipetting a drop of pure water on the hydrogel. (G–I) AFM height images of the different areas of the hydrogel (denoted by the squares in (F)). (G) corresponds to the square i. (H) corresponds to the square ii. The arrow in (H) indicates the melting of scaffold. (I) corresponds to the square iii. (J) Higher resolution AFM height image (the scan area is denoted by the square in (I)). (K,L) AFM height images of the degraded hydrogel washed by the second drop of water. (M,N) AFM height image (M) and AFM deflection image (N) of the degraded hydrogel washed by the third drop of water. The circles in (M) indicate the nanoparticles.

Figure 7.
No detectable toxicity or inflammation occurs in mice after subcutaneous injection of Sundew-inspired hydrogel. (A) H&E and F4/80 IHC staining of skin from mice injected with saline, burn cream, and Sundew-inspired hydrogel. (B) Representative H&E images of multiple-tissue types from mice injected with saline, burn cream, and Sundew-inspired hydrogel ($n = 4$ per group).

Figure 8.
Sundew-inspired hydrogel encapsulating rhMG53 formulation improves dermal wound healing in mice. (A) Cutaneous wounds were subcutaneously applied with saline, rhMG53, Sundew-inspired hydrogel, or Sundew-inspired hydrogel+rhMG53. (B) Excisional wounds images at different time points in mice receiving saline, rhMG53, Sundew-inspired hydrogel, or Sundew-inspired hydrogel +rhMG53. (C,D) Qualification of the wound closure following excisional wounding. (C) Sundew-inspired hydrogel treatment enhanced wound healing as compared to the saline control at day 5 and day 7, and (D) the treatment with Sundew-
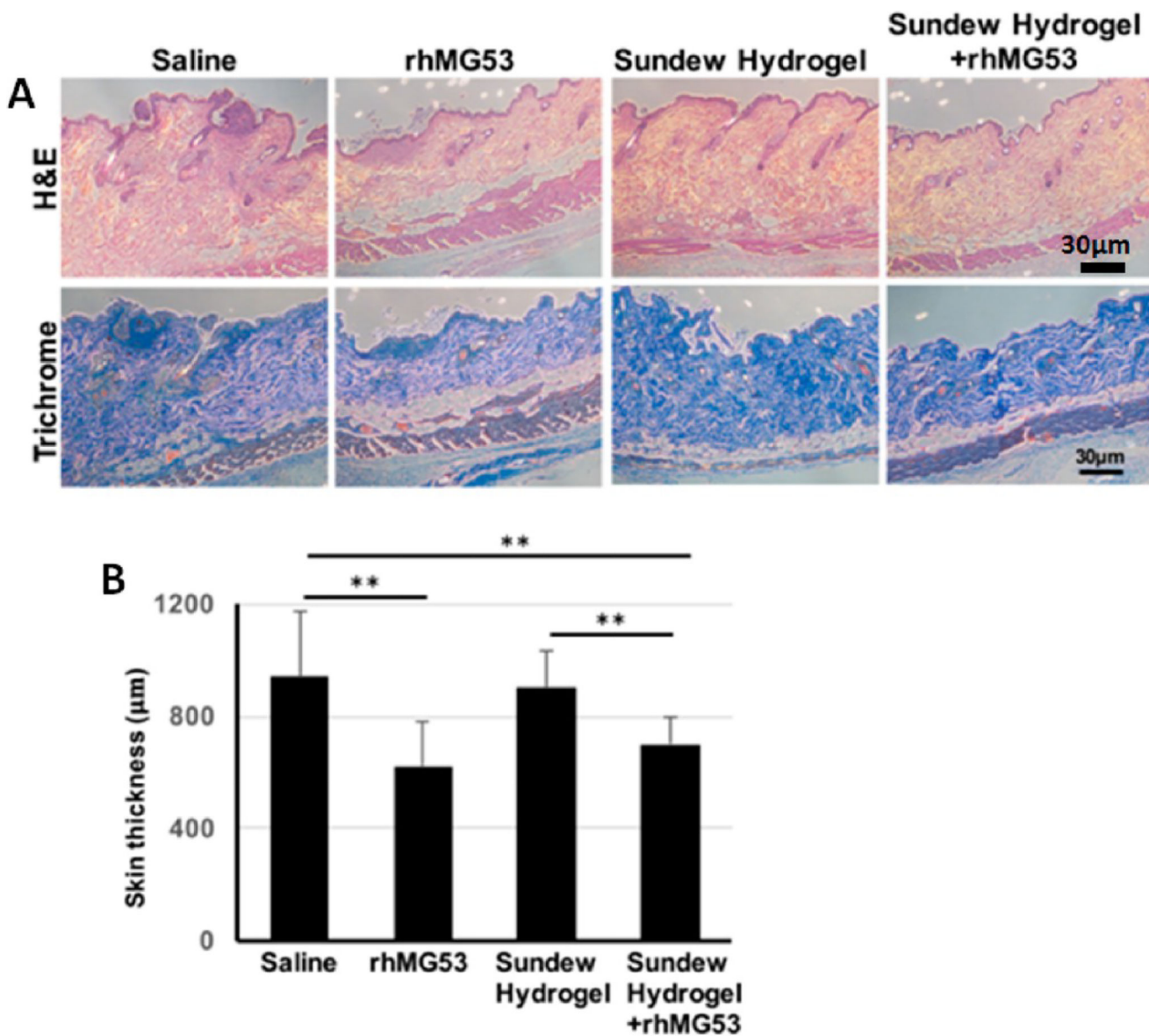
inspired hydrogel encapsulating rhMG53 significantly enhanced healing at day 5 and day 7 as compared to saline or rhMG53 treatment alone (mean ± SD; **$P < 0.01$, $n = 6$ per group).

Figure 9.
Sundew-inspired hydrogel encapsulating rhMG53 reduces skin scar formation. (A) Excisional wounds of mice were treated with saline, rhMG53, Sundew-inspired hydrogel, or Sundew-inspired hydrogel encapsulating rhMG53. Representative macroscopic H&E (top panels) and Masson's trichrome staining (bottom panels) images of the skin were taken at day 30 after injury. Images show decreased skin scar formation (collagen deposition, staining in blue). (B) Quantification of skin thickness in wound site on day 30 following excisional wounding from the mice treated with saline, rhMG53, Sundew-inspired hydrogel, or Sundew-inspired hydrogel encapsulating rhMG53 (mean ± SD; $**P < 0.01$, $n = 4$ per group).